Ariel E. Marcy, Thomas Guillerme, Emma Sherratt, Kevin C. Rowe, Matthew J. Phillips, and Vera Weisbecker

Australian Rodents Reveal Conserved Cranial Evolutionary Allometry across 10 Million Years of Murid Evolution

The American Naturalist, 2020; 196(6):755-768

Australian rodents reveal conserved Cranial Evolutionary Allometry across 10 million years of murid evolution

Ariel E. Marcy[1*], Thomas Guillerme[2], Emma Sherratt[3], Kevin C. Rowe[4,5], Matthew J. Phillips[6], and Vera Weisbecker[1,7]

[1]University of Queensland, School of Biological Sciences; University of Sheffield, Department of Animal and Plant Sciences; [3]University of Adelaide, School of Biological Sciences, [4]Museums Victoria, Sciences Department; [5]University of Melbourne, School of BioSciences; [6]Queensland University of Technology, School of Biology & Environmental Science; [7]Flinders University, College of Science and Engineering; *aemarcy@gmail.com

Keywords: allometric facilitation, CREA, geometric morphometrics, molecular phylogeny, Murinae, stabilizing selection

ABSTRACT

Among vertebrates, placental mammals are particularly variable in the covariance between cranial shape and body size (allometry), with rodents a major exception. Australian murid rodents allow an assessment of the cause of this anomaly because they radiated on an ecologically diverse continent notably lacking other terrestrial placentals. Here we use 3D geometric morphometrics to quantify species-level and evolutionary allometries in 38 species (317 crania) from all Australian murid genera. We ask if ecological opportunity resulted in greater allometric diversity compared to other rodents, or if conserved allometry suggests intrinsic constraints and/or stabilizing selection. We also assess whether cranial shape variation follows the proposed "rule of craniofacial evolutionary allometry" (CREA), whereby larger species have relatively longer snouts and smaller braincases. To ensure we could differentiate parallel versus non-parallel species-level allometric slopes, we compared the slopes of rarefied samples across all clades. We found exceedingly conserved allometry and CREA-like patterns across the 10 million year split between *Mus* and Australian murids. This could support both intrinsic constraints and stabilizing selection hypotheses for conserved allometry. Large-bodied frugivores evolved faster than other species along the allometric trajectory, which could suggest stabilizing selection on the shape of the masticatory apparatus as body size changes.

Introduction

Allometry, or the scaling relationships between physical traits as body size changes, greatly impacts and often constrains the evolution of animal morphological diversity (Huxley and Teissier 1936; Pélabon et al. 2014). Related species with different body sizes usually have morphologies close to those predicted by their clade's evolutionary allometric trajectory, even when natural selection would favor alternative scaling relationships (Pélabon et al. 2014; Serb et al. 2017). Therefore, evolutionary allometry represents a compromise between the natural selective regimes driving diversification and the clade's inherited development underlying morphology (Voje et al. 2014). Placental mammals show exceptional variation in size and morphology and thus offer an intriguing case to explore this compromise between extrinsic selection and intrinsic development (Tsuboi et al. 2018). Indeed, the unique placental pregnancy appears to provide a developmental environment that increases the viability of early developmental variations compared to other vertebrates, including other mammals (Lillegraven 1974; Millar 1977). In turn, greater allometric diversity provides natural selection with more morphological diversity to target, which could facilitate both rapid allometric divergence (Esquerré et al. 2017) and increased speciation in placentals (Jungers 1982; Schluter 1996; Wund et al. 2012; Marcy et al. 2016).

Given their extremely high speciosity, rodents show unusually low morphological diversity (Hautier and Cox 2015), which appears to be a result of their low rates of allometric evolution compared to other mammals (Venditti et al. 2011). Muridae, a single rodent family, includes 12.8% of all mammalian species but their morphology appears to

follow a highly conserved allometric pattern (Fabre et al. 2012; Burgin et al. 2018), especially within the cranium (Firmat et al. 2014; Verde Arregoitia et al. 2017; Alhajeri and Steppan 2018). The unexpected allometric conservatism of murid rodents positions them as model organisms for understanding how the interaction of extrinsic and intrinsic factors impacts allometric variation and subsequent macroevolutionary patterns.

The relative importance of extrinsic natural selection and intrinsic developmental processes on allometric patterns has long been debated (Frankino et al. 2005; Pélabon et al. 2014). Their relative importance likely exists along a spectrum, but there are three main hypotheses that attempt to define distinct, testable categories (Brigandt 2015). The first hypothesis – which most placental mammals seem to illustrate – posits that disruptive (or directional) selection can alter allometric patterns quickly, especially when a new selective pressure emerges (Frankino et al. 2005; Tsuboi et al. 2018). This "extrinsic pressure hypothesis" expects changes in selection to be the most important determinant of the allometric patterning for a given species or clade. At the opposite end of the spectrum, the second hypothesis emphasizes how conserved allometric patterns arise from inherited developmental processes (Voje et al. 2014). This "intrinsic constraint hypothesis" posits that allometry stays conserved because genetic changes to development have pleiotropic effects and thus expects allometry to be limited to the few viable variations (Marroig and Cheverud 2010; Shirai and Marroig 2010). The intermediate hypothesis posits that the interaction of extrinsic stabilizing selection (a subcategory of natural selection) on intrinsic development produces consistently functional morphologies (Marroig and Cheverud 2005). Unlike the extrinsic pressure hypothesis, this "stabilizing selection hypothesis" expects outcomes similar to – perhaps

even indistinguishable from—the intrinsic constraint hypothesis (Brigandt 2015). Notably, the stabilizing selection hypothesis expects that sustained stabilizing selection on limited viable genetic variation could hone an allometric trajectory that facilitates a clade's rapid radiation (Marroig and Cheverud 2005; Voje et al. 2014; Cardini et al. 2015). This so-called "allometric line of least resistance" is thought to scale stable, functional morphological ratios for a wide range of body sizes (Schluter 1996).

The allometric patterning of Australian murid rodents could plausibly be characterized by each of the three hypotheses. First, their radiations would have experienced new extrinsic selection pressures by immigrating from wet tropics onto a much drier continent (Aplin and Ford 2014; Smissen and Rowe 2018). Indeed, unlike nearly all other murid radiations, the Australia-New Guinea radiations show some evidence of following an ecological opportunity model (*sensu* Yoder et al. 2010), where adaptation to new environments, especially the dry habitats, could be driving speciation (Schenk et al. 2013; Smissen and Rowe 2018; but see Alhajeri et al. 2016). Furthermore, Australia uniquely lacks other terrestrial placental mammals (Aplin and Ford 2014), therefore it is possible that a release from competition could allow extrinsic pressures to push murid rodent allometry into morphological niches unavailable to all other murids. However, in order for extrinsic pressures to be the main determinant of allometric patterns, murids would need to arrive in Australia with flexible developmental processes. Evidence for conserved allometry in murids in general (Porto et al. 2013; Firmat et al. 2014) makes the extrinsic pressure selection hypothesis appear unlikely for Australian murids.

Additional understanding on the intrinsic factors influencing allometry in mammals can come from assessments of allometry-related shape variation patterns. Many major mammalian clades have conserved shape patterns that follow the proposed "rule" for craniofacial evolutionary allometry (CREA *sensu* Cardini et al. 2015), where larger species have relatively longer snouts and smaller braincases compared to smaller species (Radinsky 1985; Cardini and Polly 2013; Cardini et al. 2015; Tamagnini et al. 2017; Cardini 2019). CREA does not yet have a satisfactory explanation (Cardini 2019), but this conserved allometric pattern could be attributed to post-natal growth patterns instrinsic to both marsupial and placental mammals (Cardini et al. 2015). If CREA is present in rodents, it could also possibly be explained by the stabilizing selection hypothesis because cranial allometry could scale the function of their derived masticatory apparatus for gnawing (Alhajeri and Steppan 2018). The apparatus includes actively sharpened incisors, a diastema allowing independent occlusion at the incisors or at the molars, and a craniomandibular joint allowing movement between occlusion points (Druzinsky 2015). This complexity would decrease viability of developmental alterations since any maladaptive ratios would decrease fitness and simultaneously reinforce an allometric line of least resistance. However, many murid dietary specialists diverge in mandible shape (Renaud et al. 2007; Esselstyn et al. 2012; Fabre et al. 2017). These specialists indicate an interesting threshold between stabilizing and other forms of natural selection, which suggests the latter can shift long-standing allometric patterns to accommodate new masticatory biomechanics. Therefore, exceptions to the allometric "rules" may provide insight into the conditions leading to large adaptive leaps,

such as a population entering a new selection regime, evolving a genetic mutation that lifts a constraint, or both (e.g. Polly 2008; Cardini et al. 2015).

Australian murid rodents represent at least eight recent and relatively rapid radiations with high species richness and diverse ecological adaptations, including dietary and locomotor specializations (Rowe et al. 2008; Aplin and Ford 2014). In this study, we use 3D geometric morphometric analyses to assess their cranial allometry and morphology within and among 38 species, covering 58% of species and all genera extant on modern-day Australia (fig. 1). Specifically, we ask three questions: First, are there divergent allometric patterns, consistent with the ecological opportunity model of a predominant role for extrinsic pressures on Australian murid rodent allometry? Second, if allometry is conserved, does it follow suggested deeply conserved mammalian shape patterns like CREA? Third, if allometry is conserved, is there evidence for stabilizing selection, in particular an “allometric line of least resistance” facilitating species to rapidly evolve functional shapes along the common evolutionary allometric trajectory?

Methods

Data Collection: Shape and Size Data

We sampled crania from four Australian museums: Queensland Museum (Brisbane), Australian Museum (Sydney), South Australian Museum (Adelaide), and Museums Victoria (Melbourne). The 317 adult specimens represent 35 species of native and 3 species of invasive rodents, including all 14 extant genera of rodents in Australia. Adults were determined by an emergent third molar and closure of the basisphenoid-basioccipital suture. When possible, species were represented by 10 individuals, 5

males and 5 females (see table S1). Each cranium was scanned with a HDI109 blue light surface scanner (LMI Technologies Inc., Vancouver, Canada) on a rotary table. We followed the same scanning method as Marcy et al. (2018). Note that our scanner's resolution was insufficient to capture the very thin lateral zygomatic arches of smaller specimens, which we accepted as a trade-off for the large number of specimens acquired. This was deemed appropriate because skeletonization would have caused specimen preparation error as the fine structure dried and lost support from surrounding muscles (Yezerinac et al. 1992; Schmidt et al. 2010). The rest of the crania, including the roots of the zygomatic arches and main areas of muscle attachment (i.e. massetaric scar and temporal fossa), was captured.

3D crania scans were landmarked in Viewbox version 4.0 (dHAL software, Kifissia, Greece; www.dhal.com (Polychronis et al. 2013)). A preliminary analysis of all genera using the landmarking template from Marcy et al. (2018) identified the eastern chestnut mouse, *Pseudomys gracilicaudatus* (Gould, 1895) QM-JM9681 as the mean specimen, which was used to create a new template. In the present study, crania were characterized by 60 fixed landmarks, 141 curve semi-landmarks, and 124 patch semi-landmarks for a total of 325 landmarks (table S2 and fig. S1). The fixed landmarks do not slide, the curve semi-landmarks slide along a user-defined curve, and the patch semi-landmarks slide across a surface bounded by curves. Sliding was done in Viewbox by minimizing bending energy from 100% to 5% exponential energy over six cycles of projection and sliding.

During landmarking the mesh was rotated and/or the virtual lighting was changed to locate each landmarks' position. The specimens were landmarked in a random order

by one person (AEM) to avoid inter-observer error (Fruciano et al. 2017). The first 20 specimens were removed to reduce user error prior to learning the template. Another 20 specimens were digitized twice to assess observer error. Once landmarking was complete, large landmarking errors were identified and corrected with the *plotOutlier* function in *geomorph* (v.3.0.7) (Adams, Collyer, and Kaliontzopoulou 2018). Repeatability for the main dataset was about 93%, which is standard user error for 3D geometric morphometrics (e.g. Fruciano 2016; Fruciano et al. 2017; Marcy et al. 2018).

The landmark coordinates were prepared for statistical analysis using a generalized Procrustes analysis – removing differences in size, position, and orientation, leaving only shape variation (Rohlf and Slice 1990) – in R (v.3.6.1) (R Core Team 2019) and *geomorph* (v.3.1.0) (Adams et al. 2019). Afterwards, each cranium retains an associated centroid size as a proxy of body size (calculated as the square root of the sum of the squared distance of every landmark to the centroid or "center" of the landmark configuration (Zelditch et al. 2004)). The processed coordinates were used as shape variables for the following geometric morphometric, allometric, and phylogenetic analyses. While some reviews have criticized geometric morphometrics for using Gould-Mosimann allometry over the original Huxley-Jolicoeur framework (Pélabon et al. 2014; Voje et al. 2014), both frameworks are logically compatible and unlikely to yield contradictory results (Klingenberg 2016).

Data Collection: Time-Calibrated Phylogenetic Tree

The phylogenetic tree (see fig. 1) for murid rodent species represented by 3D surface scans was compiled from DNA sequences from ten previously sequenced genes: a

mitochondrial protein coding locus (cytochrome b) and 9 nuclear exons (exon 1 of ADRA2B, exon 9 of ARHGAP21, exon 11 of BRCA1, exon 8 of CB1, exon 10 of GHR, exon 1 of IRBP, the single exon of RAG1, exon 7 of TLR3, and exon 29 of vWF). Using the alignments of Smissen and Rowe (2018) as our starting point, we removed extraneous taxa and added taxa to obtain an alignment including 72 murid species in subfamily Murinae (table S3). These included all but two of the 38 species in our morphological dataset. No sequences were available for the central rock-rat, *Zyzomys pedunculatus* (Waite, 1896) or for Australia's undescribed species of *Pogonomys* (Milne-Edwards, 1877). However, for our analyses we used the New Guinean large tree mouse, *Pogonomys loriae* (Thomas, 1897) as a surrogate as the two species are equidistant from other taxa in our analyses. Additional species were included as outgroups and for fossil-calibration (see table S3).

With our concatenated alignment of 10 loci and 72 species, we estimated a time-calibrated ultrametric phylogeny using a relaxed molecular clock approach in BEAST (v.2.1.3) (Bouckaert et al. 2014). Appropriate DNA sequence partitions and substitution models were found following settings as were a total of four calibration points specified in Smissen and Rowe (2018). These combine three fossils from the Siwalik Formation (Kimura et al. 2015) with a calibration for the origin of Australian murines (Aplin and Ford 2014). We applied a Yule speciation prior and set the birthrate prior to exponential with an initial mean of 10. Other priors were left at default settings. Initial runs were used to optimize operators and we conducted a final Markov Chain Monte Carlo run with 2×10^8 generations, sampling trees and other parameters every 2000 generations. We evaluated convergence and assessed sampling adequacy in Tracer (v.1.4)

(Rambaut and Drummond 2007). TreeAnnotator was used to discard the first 20% of trees as burn-in and pool the remaining samples to form the posterior distribution and generate a maximum clade credibility tree. Finally, we manually pruned the resultant tree to the 37 species. The most recent phylogeny shows the broad-toothed rat, *Mastacomys fuscus* (Thomas, 1882) falling within genus *Pseudomys* (Smissen and Rowe 2018) so we placed this species in *Pseudomys* for analyses.

Allometric Variation

To address all three questions and characterize allometric patterns in Australian murids, we tested allometric variation at three levels: static allometry (species-level), evolutionary allometry (among clades), and a phylogenetic rarefaction testing every node in the tree.

First, variation in static (species-level) allometries was tested using an analysis of covariance (ANCOVA) model, implemented with *geomorph* function *procD.lm* (for highly-multivariate data), and evaluated for significance with Goddall's (1991) F-test with 500 permutations. A post-hoc test using package *RRPP* (v.0.4.3) (Collyer and Adams 2018, 2019) function *pairwise* evaluated whether the static allometric slopes of all species (n = 38) significantly differ from one another. Multiple comparisons were accounted for by reducing alpha to 0.01. The model was visualized by plotting the regression scores of shape on size versus log centroid size (Drake and Klingenberg 2008).

Second, variation in evolutionary (among clades) allometries was tested using an ANCOVA model similar to the above. Howevever, instead of species, six major clades

were defined as a radiation from an ancestor that arrived in Australia at a distinct time, after Aplin and Ford (2014) plus monospecific lineages for house mouse *Mus musculus* (Linneaus, 1758) and large tree mouse *Pogonomys* sp. (see fig. 1). We also compared these results with a phylogenetic ANCOVA (pANCOVA) using *geomorph*'s *procD.pgls* (Adams 2014), which excutes the ANCOVA model in a phylogenetic framework. This pANCOVA used mean centroid sizes from all 37 species included in the tree.

One analytical challenge – even with our comparatively large sample sizes – is that available specimens per species may be too small to confidently estimate species-level allometric slopes. Therefore, we developed a new function, *rarefy.stat* in *landvR* (v.0.4) (Guillerme and Weisbecker 2019) and modified the *prop.parts* function from *ape* (v.5.2) (Paradis and Schliep 2018) to estimate how well our calculations of species-level allometric slopes withstood downsampling relative to the larger clade-level allometric slopes. We used this phylogeny-based rarefaction to assess whether our sampling effort could support our interpretations.

To conduct phylogenetic rarefaction on static allometric slopes, we first measured the observed allometric slope for every clade in figure 1, from the entire dataset to each individual species. Then we removed all but five random specimens (our smallest species sample size) from each clade and re-measured this rareified allometric slope, repeated 100 times. The median slope change between the random sample and the slope across the whole clade was calculated from the 100 values created by subtracting the observed slope from each rarefied slope in each clade. We calculated the absolute median slope change in degrees for each clade using the trigonometric formula for the angle between two slopes. We considered the rarefied

slope to be significantly different to the observed slope if their angle was higher than 4.5° (5% of 90° – the largest possible angle between the two slopes). We visualized the results using a boxplot showing the 95% and 50% confidence intervals of the delta slope values and a scatterplot of the delta slope angles in context with the 4.5° confidence line. To ensure our results were not biased by close phylogenetic relationships, we randomly assigned species into groups with the same number of species as each clade in the phylogeny and reran the analysis above. We repeated this analysis for 100 different sets of random groups, ignoring single-species clades. Results were visualized using a boxplot of the median delta slopes.

CREA Shape Patterns

To address our second question on craniofacial evolutionary allometry (CREA) we assessed size and shape covariation using three types of plots. First, we used *geomorph*'s *procD.lm* to plot the evolutionary allometric relationship between log centroid size versus the regression of shape on size (Drake and Klingenberg 2008). Second, we used *geomorph*'s *plotTangentSpace* to plot a principal components analysis (PCA) to provide a "size-less" morphospace comparison of the mean shapes for each species. Third, we visualized the cranial shape variation across the minimum and maximum values of principal component (PC)1 using landmark heatmaps produced by *landvR* function *procrustes.var.plot* (Guillerme and Weisbecker 2019; Weisbecker et al. 2019). The heatmaps allowed us to determine whether the shape variation pattern resembled CREA (Cardini et al. 2015).

Rates of Shape Evolution

To address our third question on stabilizing selection and facilitation, we used an evolutionary allometry plot to identify two types of outliers: large-bodied specialists on the common allometric line as well as specialists diverging from it. While specialists for frugivory, carnivory, and hopping locomotion are relatively easy to define, folivores exist along a spectrum. We identified our three "specialist folivore" species based on descriptions of craniodental modifications for folivory (e.g. broadened and/or high-crowned molars) and on field studies demonstrating diet dependence: the broad-toothed rat, *Mastacomys fuscus,* the Hastings River mouse, *Pseudomys oralis* (Thomas, 1921), and the greater stick-nest rat, *Leporillus conditor* (Sturt, 1848) (Watts and Braithwaite 1978; Fox et al. 1994; Murray et al. 1999; Ryan et al. 2003; Breed and Ford 2007). Using the mean shapes and the phylogeny of 37 species we ran *geomorph*'s *compare.evol.rates* to find pairwise comparisons of shape evolution rates between specialists and between specialists to non-specialists. The Bonferroni correction accounted for multiple comparisons (Bonferroni 1936).

All specimen surface files for Australian rodent crania included in this study are publicly available for unrestricted download from MorphoSource Project 561: http://www.morphosource.org/Detail/ProjectDetail/Show/project_id/561 (Marcy 2018). All data needed to reproduce the figures and tables are deposited in GitHub: https://github.com/miracleray/allometry-rodents and in the Dryad Digital Repository: https://doi.org/10.5061/dryad.z8w9ghx91 (Marcy et al. 2020).

Results

Allometric variation

At the static allometry level, the ANCOVA indicates that size accounts for a large fraction (36.5%) of shape ($R^2 = 0.365$, $p < 0.002$), only slightly less than the variation explained by species affiliation ($R^2 = 0.405$, $p < 0.002$) (table 1). The post-hoc test for homogeneity of slopes found that, out of 703 pairwise comparisons, only nine had significant differences in slopes (table S4). The New Holland mouse, *Pseudomys novaehollandiae* (Waterhouse, 1843) had the greatest number of significant pairwise differences with six (out of a possible 37). All other species with significant pairwise differences had less than three such comparisons (table S4). Together, the ANCOVA and the homogeneity of slopes tests reject the extrinsic pressure hypothesis for ecological opportunity in Australia. Instead they support conserved allometry in which murid rodent species have parallel static allometric slopes (fig. 2).

Second, the evolutionary allometry (among clades) ANCOVA also showed a high R^2 term for size ($R^2 = 0.364$, $p < 0.002$), about twice that of clade ($R^2 = 0.175$, $p < 0.002$), indicating a conserved allometric signal across the phylogeny (table 2). The ANCOVA also revealed a small yet significant interaction term between clade and log centroid size (table 2). This interaction term means that evolutionary allometric slopes differ slightly among clades. However, the coefficient of determination (R^2) of this interaction is small: it only accounted for 5.6% of variation, compared with 37% and 18% for log centroid size and clade, respectively (table 2). The pANCOVA of mean shapes against size returned similar results, with size accounting for 41% of variation. While the interaction term (table S5, $R^2 = 0.134$, $p < 0.02$) is higher in this analysis, it

uses fewer data points (mean shapes). Note that in both analyses, the species-rich Pseudomys division (*sensu* Smissen and Rowe 2018, which uses roman font to distinguish the larger clade from the genus) (n = 19 species) may introduce some sampling bias relative the other clades (n = 1-6 species).

Figure 2*A* illustrates the evolutionary allometry (grey line), which is shallower than static allometries but is correlated with the overall trend of size and shape across all species (table 1, R^2= 0.36, $p < 0.002$). This pattern occurs when slopes stay constant and species vary only slightly in y-intercepts (Pélabon et al. 2014). Here, y-intercepts generally decrease with increasing body size, which generates the shallower evolutionary allometry slope.

Third, phylogenetic rarefaction supports that our sampling is sufficient to reject a hypothesis of non-parallel slopes by showing that the conserved allometric trends found at the species and clade levels persist at a low sample size (n = 5) across each node of the tree (fig. 3). All clades had a median delta slope change less than 2.6 relative to the all-clade slope (fig. 3*A*), when converted to degrees, this corresponds to 93% of clades (67 of 73) remaining under the conservative 4.5° cut-off for slope angle change (fig. 3*B*). Randomizing the phylogeny did not change these results (fig. S2). Larger clades have much larger sample sizes to begin with, yet their median slope angles did not change significantly when downsampled. Therefore, we conclude that sample sizes of 5 or greater are sufficient for our study.

Craniofacial Evolutionary Allometry (CREA)

Consistent with the ANCOVAs, the evolutionary allometry plot shows few species diverging from the common evolutionary allometric trajectory (fig. 4*A*), establishing that a conserved pattern of cranial allometry exists in Australian rodents. The first two PC axes of the PCA represent 67% of the mean species shape variation (52.3% PC1, 14.5% PC2) while remaining PCs each explained 8.0% of variation or less (the first 10 PCs had a proportion of variance >1% each). Most of the shape variation, as identified by PC1 (fig. 4*B*), relates to allometry, with most species falling in the same order along the x-axes of centroid size and PC1 (fig. 4*A,B*). The PC1 landmark heatmaps clearly illustrate the PC1 minimum cranium having a larger basicrania and shorter snout compared to the mean shape (fig. *4C,D*) and the PC1 maximum cranium showing the opposite trend (fig. *4E,F*). These shapes are fully consistent with CREA (Cardini and Polly 2013; Cardini et al. 2015; Tamagnini et al. 2017).

Specialist species that diverge from the allometry plot also diverge from the main cluster of more generalist species along PC2 in the PCA (fig. 4*A,B*). Folivorous specialists score highest on PC2 (fig. 4*B*, dark purple circle, blue open triangle and quartered circle) while carnivorous specialists score lowest on PC2 (fig. 4*B*, dark red and red circles).

Rates of shape evolution

Two frugivores – the black-footed tree rat, *Mesembriomys gouldi* (Palmer, 1906) and the giant white-tailed rat, *Uromys caudimaculatus* (Krefft, 1867) – independently evolved large bodies and outlying cranial shapes along PC1. In doing so, both species

evolved along the common evolutionary allometric trajectory (fig. 4*A,B*). Of the three folivores, only the Hastings River mouse, *P. oralis* and the broad-toothed rat, *M. fuscus*, diverge along PC2 and from the common evolutionary allometric trajectory (fig. 4). The third folivore, the greater stick-nest rat, *L. conditor* falls directly along the allometric trajectory (fig. 4). Both carnivores diverge along common evolutionary allometry trajectory and along PC2 with the opposite loading from the folivores (fig. 4*A,B*). The water rat, *Hydromys chrysogaster* (Geoffrey, 1804) appears most divergent from the common evolutionary allometry trajectory (fig. 4*A*). The bipedal hopping *Notomys* appear to have an among-clade allometry that diverged in y-intercept but not in slope from other, predominantly quadrupedal Australian rodents (fig. 4*A*). They consistently show low PC1 scores (fig. 4*B*).

Pairwise analysis of shape evolution rates revealed that crania of large-bodied frugivores evolved 4.6 times faster than those of non-specialists (table S6, $p = 0.02$). The two frugivores evolved on the common evolutionary allometric trajectory independently, supporting the hypothesis for facilitation along a line of least resistance, an outcome of stabilizing selection. The three folivores also evolved faster than non-specialists (3.0 times faster, $p = 0.02$) even though two species appear to diverge from the common allometric trajectory. All other pairwise comparisons were non-significant, including for specialists diverging from the common evolutionary allometry trajectory (table S6, $p > 0.05$).

Discussion

We find strong, conserved allometry of skull shape across nearly all levels of the Australian murid rodent phylogeny, explaining substantial amounts of the variation (roughly 40% of both the static (species-level) and evolutionary variation as well as over half (52%) of variation along PC1). We therefore find no support for the extrinsic pressure hypothesis (that there should be divergence of allometric slopes because of divergent selection pressures). In fact, with very few exceptions, all species retain a similar allometric slope across divergences as wide as ten million years – since the split between *Mus* and the clade including all native Australian rodents (Aghová et al. 2018). Our new phylogeny-based rarefaction, bootstrapping, and randomization method shows that this allometric conservation transcends taxanomic boundaries across the entire sample, with nearly no significant differences between static and evolutionary allometric slopes. Indeed, static allometric slope angles showed almost no significant changes between samples, even when species from different clades were combined at random. The strict conservation of allometric scaling is particuarly striking for such a speciose group encompassing six major radiations onto a new continent with novel environments (Yoder et al. 2010; Aplin and Ford 2014). While strongly conserved allometry has been detected among closely related species (Singleton 2002; Cardini et al. 2015; Munds et al. 2018), we are not aware of similar levels of allometric conservation across any other large radiation of mammals. Our results therefore demonstrate rodents to be an example of extreme allometric conservatism within the placentals, a clade otherwise thought to have a high degree of evolvability in cranial allometry (Tsuboi et al. 2018).

Our heatmap visualizations of both allometric and ordinated (PCA) shape variation demonstrate that the high degree of allometry in Australian murids coincides with shape variation known as “craniofacial evolutionary allometry” (CREA). CREA is found across diverse mammalian lineages, and describes allometric shape variation where larger species have relatively longer snouts and smaller braincases compared to related species with smaller body sizes (Cardini and Polly 2013; Cardini 2019). However, due to their particularly conserved allometry, Australian murid rodents appear to be uniquely constrained to CREA compared to other mammals.

The underlying cause of CREA across Mammalia is still under investigation (Cardini 2019). Current hypotheses include developmental constraints as well as persistent selection on function via stabilizing selection (Cardini and Polly 2013). The instrinsic constraint hypothesis is certainly supported by the finding that murid rodents, with fast reproduction and altricial neonates compared to other placentals, would have shape evolution driven primarily by size (Porto et al. 2013). Furthermore, Australian murids vary in reproductive rate by clade, with the highest reproductive rates occuring in the most morphologically conserved clade of native *Rattus* (Yom-Tov 1985; Geffen et al. 2011; Rowe et al. 2011). Therefore, our results position Australian murid rodents as potentially developmentally-constrained exceptions to the placental pattern, supporting the general hypothesis for increased morphological diversity in clades of placentals with longer relative gestations than rodents (Porto et al. 2013; Tsuboi et al. 2018).

Despite the strong indication of a developmental constraint, constraint hypotheses are not mutally exclusive with hypotheses of stabilizing selection. Indeed, we found complimentary lines of evidence that support a strong role for stabilizing

selection. In particular, stabilizing selection can act on available genetic variation to produce an allometric line of least resistance that scales viable and functional morphological ratios with body size (Schluter 1996). In our dataset, two frugivores from different radiations evolved large body sizes with similar cranial shapes that sit along the evolutionary allometry trajectory; this was accompanied by significantly faster rates of shape evolution compared to non-specialists. Faster evolution is predicted under the stabilizing selection hypothesis because of facilitation by the allometric line of least resistance (Schluter 1996; Marroig and Cheverud 2005). This appears to be a likely scenario for Australian large-bodied frugivores because experimental work has suggested that the general murid gnawing apparatus maintains frugivory with few or no changes (Cox et al. 2012; Maestri et al. 2016).

We can also make a case for the existence of stabilizing selection in Australian murids by examing the folivores and carnivores. These two groups deviated from the common allometric line and in the PCA. Two folivores, *M. fuscus* and *P. oralis*, showed higher PC2 values corresponding to broader molars than non-folivorous species of the same size. In contrast, carnivores showed lower PC2 scores, with fewer teeth and a rostrum morphology adaptive for capturing prey; an unusual niche for rodents (Fabre et al. 2017). These morphological changes did not alter the conserved species-level allometric slope, even for carnivorous water rat, *Hydromys chrysogaster,* whose mean projected shape to size ratio falls noticeably above the common evolutionary allometric trajectory. It is possible that adaptations away from the common evolutionary allometric line come with trade offs. For example, an anatomical study of *H. chrysogaster* suggested that they maximize bite force by reducing movement at their

craniomandibular joint (Fabre et al. 2017). However, this adjustment reduces the independent occlusion of molars and incisors characteristic of most murids (Druzinsky 2015). In *H. chrysogaster,* molar occlusion during chewing appears to cause maladaptive microwear on the incisors that results in breakage (Fabre et al. 2017). This trade-off suggests that disruptive selection can occur in Australian rodents, but that stabilizing selection on the murid gnawing apparatus acts as a strong antagonist to changes away from the evolutionary allometric line.

Australian murid rodents can be compared to many other mammalian radiations with regards to allometry and conserved morphology. For example, Indo-Australian murid rodents evolved carnivory five times (Rowe et al. 2016) and South-East Asian murid vermivores evolved unusual crania that appear to diverge from CREA (Esselstyn et al. 2012; Rickart et al. 2019). These relatives could be used to explore how disruptive or directional selection could overpower previously existing stabilizing selection. Indeed, the intense stabilizing selection that we infer acts on the complex gnawing apparatus of rodents invites comparisons to the unrelated clade of multituberculates, which share features of this apparatus (Lazzari et al. 2010). This combination of characters appears to correspond with similar patterns of low cranial diversity, high species richness, and success in a range of environments (Lazzari et al. 2010). Indeed, clades with low morphological diversity could have a highly adaptive suite of morphological ratios whose biomechanics scale along an allometric line (Marroig and Cheverud 2005; Cardini and Polly 2013). In these cases, non-allometric morphological diversity would be determined by intrinsic constraints and how much deviation from existing allometry is tolerated by stabilizing selection (Estes and Arnold 2007). New World monkeys show allometric

patterns suggestive of both constraint and stabilizing selection, with evidence that the latter could have facilitated evolution along a line of least resistance (Marroig and Cheverud 2005, 2010). This clade would provide an ideal comparison to altricial Australian murids to disentangle these two factors further because monkeys – unlike murids – have slow reproductive rates, like most other placental clades (Lillegraven 1974; Porto et al. 2013; Tsuboi et al. 2018).

Conclusions

Understanding the specific roles of intrinsic constraints and stabilizing selection on conserved allometric patterns like CREA has the potential to answer fundamental macroevolutionary questions (Cardini 2019). However, the conceptual difference is difficult to disentangle because, as our study shows, CREA appears to be a long-term emergent property of both genetics and selection (i.e. it represents the compromise between instrinsic developmental programs and extrinsic selection on viable forms throughout ontogeny) (Pélabon et al. 2014; Brigandt 2015). Measuring ontogenetic allometry could eliminate intrinsic constraints as the limiting factor if high ontogenetic variation exists, indicating a larger role for stabilizing selection (Jamniczky and Hallgrímsson 2009). There is already some evidence that murid rodents have highly variable ontogenetic allometry despite conserved static allometries (Wilson and Sánchez-Villagra 2009). Finally, the trade-off observed between conserved allometric shape and orthogonal shape variation deserves further exploration as a possible avenue to understand the interaction between factors influencing allometry and total morphological variation.

Acknowledgements

We thank Dr Heather Janetzki for hosting AEM many times in the mammal collections at the Queensland Museum, Laura Cook for hosting at the Museum Victoria, Dr Sandy Ingleby for hosting at the Australian Museum, and Dr David Stemmer for loaning specimens from the South Australian Museum. Thanks to lab assistants Lauren Thornton and Aubrey Keirnan for help uploading 3D meshes to Morphosource. We also thank Editor Dan Rabosky and two anonymous reviewers for their insightful comments that greatly enhanced the manuscript. This work was funded by Discovery Grant DP170103227 to VW and MJP, as well as by a School of Biology Postgraduate Travel grant to AEM.

Author Contributions

Conceptualized by AEM and VW; data collection by AEM and KCR; methods development by TG, AEM, and VW; data analysis and visualization by AEM, TG, ES and KCR; writing – original draft by AEM and VW; writing – review & editing by VW, AEM, KCR, TG, ES, and MJP; supervision and funding acquisition by VW and MJP.

Literature Cited

Adams, D. C. 2014. A method for assessing phylogenetic least squares models for shape and other high-dimensional multivariate data. Evolution 68:2675–2688.

Adams, D. C., M. L. Collyer, and A. Kaliontzopoulou. 2018. *geomorph*: Software for geometric morphometric analyses. R package version 3.0.7.

——— 2019. *geomorph*: Software for geometric morphometric analyses. R package version 3.1.0.

Aghová, T., Y. Kimura, J. Bryja, G. Dobigny, L. Granjon, and G. J. Kergoat. 2018. Fossils know it best: Using a new set of fossil calibrations to improve the temporal phylogenetic framework of murid rodents (Rodentia: Muridae). Molecular Phylogenetics and Evolution 128:98–111.

Alhajeri, B. H., J. J. Schenk, and S. J. Steppan. 2016. Ecomorphological diversification following continental colonization in muroid rodents (Rodentia: Muroidea). Biological Journal of the Linnean Society 117:463–481.

Alhajeri, B. H., and S. J. Steppan. 2018. A phylogenetic test of adaptation to deserts and aridity in skull and dental morphology across rodents. Journal of Mammalogy 99:1197–1216.

Aplin, K., and F. Ford. 2014. Murine rodents: late but highly successful invaders. Pages 196–240 *in* H. H. T. Prins and I. J. Gordon, eds. Invasion Biology and Ecological Theory: Insights from a Continent in Transformation (1st ed.). Cambridge University Press, Cambridge.

Bonferroni, C. E. 1936. Teoria statistica delle classi e calcolo delle probabilità. Pubblicazioni del R Istituto Superiore di Scienze Economiche e Commerciali di Firenze 1–62.

Bouckaert, R., J. Heled, D. Kühnert, T. Vaughan, C.-H. Wu, D. Xie, M. A. Suchard, et al. 2014. BEAST 2: A Software Platform for Bayesian Evolutionary Analysis. PLOS Computational Biology 10:e1003537.

Breed, B., and F. Ford. 2007. Native Mice and Rats. Australian Natural History Series. CSIRO Publishing.

Brigandt, I. 2015. From Developmental Constraint to Evolvability: How Concepts Figure in Explanation and Disciplinary Identity. Pages 305–325 *in* A. C. Love, ed. Conceptual Change in Biology: Scientific and Philosophical Perspectives on Evolution and Development, Boston Studies in the Philosophy and History of Science. Springer Netherlands, Dordrecht.

Burgin, C. J., J. P. Colella, P. L. Kahn, and N. S. Upham. 2018. How many species of mammals are there? Journal of Mammalogy 99:1–14.

Cardini, A. 2019. Craniofacial Allometry is a Rule in Evolutionary Radiations of Placentals. Evolutionary Biology 46:239–248.

Cardini, A., D. Polly, R. Dawson, and N. Milne. 2015. Why the Long Face? Kangaroos and Wallabies Follow the Same 'Rule' of Cranial Evolutionary Allometry (CREA) as Placentals. Evolutionary Biology 42:169–176.

Cardini, A., and P. D. Polly. 2013. Larger mammals have longer faces because of size-related constraints on skull form. Nature Communications 4:1–7.

Cheverud, J. M. 1982. Relationships among ontogenetic, static, and evolutionary allometry. American Journal of Physical Anthropology 59:139–149.

Collyer, M. L., and D. C. Adams. 2018. *RRPP*: An R package for fitting linear models to high-dimensional data using residual randomization. Methods in Ecology and Evolution 9:1772–1779.

———. 2019. *RRPP*: Linear Model Evaluation with Randomized Residuals in a Permutation Procedure, R package version 0.4.0.

Cox, P. G., E. J. Rayfield, M. J. Fagan, A. Herrel, T. C. Pataky, and N. Jeffery. 2012. Functional Evolution of the Feeding System in Rodents. PLOS ONE 7:e36299.

Drake, A. G., and C. P. Klingenberg. 2008. The pace of morphological change: historical transformation of skull shape in St Bernard dogs. Proceedings of the Royal Society B 275:71–76.

Druzinsky, R. E. 2015. The oral apparatus of rodents: variations on the theme of a gnawing machine. Pages 323–349 *in* P. G. Cox and L. Hautier, eds. Evolution of the Rodents: Advances in Phylogeny, Functional Morphology and Development. Cambridge University Press, Cambridge.

Esquerré, D., E. Sherratt, and J. S. Keogh. 2017. Evolution of extreme ontogenetic allometric diversity and heterochrony in pythons, a clade of giant and dwarf snakes. Evolution 71:2829–2844.

Esselstyn, J. A., A. S. Achmadi, and K. C. Rowe. 2012. Evolutionary novelty in a rat with no molars. Biology Letters 8:990–993.

Estes, S., and S. J. Arnold. 2007. Resolving the paradox of stasis: models with stabilizing selection explain evolutionary divergence on all timescales. The American Naturalist 169:227–244.

Fabre, P.-H., L. Hautier, D. Dimitrov, and E. J. P Douzery. 2012. A glimpse on the pattern of rodent diversification: a phylogenetic approach. BMC Evolutionary Biology 12:88.

Fabre, P.-H., A. Herrel, Y. Fitriana, L. Meslin, and L. Hautier. 2017. Masticatory muscle architecture in a water-rat from Australasia (Murinae, *Hydromys*) and its implication for the evolution of carnivory in rodents. Journal of Anatomy 231:380–397.

Firmat, C., I. Lozano-Fernández, J. Agustí, G. H. Bolstad, G. Cuenca-Bescós, T. F. Hansen, and C. Pélabon. 2014. Walk the line: 600000 years of molar evolution constrained by allometry in the fossil rodent *Mimomys savini*. Philosophical Transactions of the Royal Society B 369.

Fox, B. J., D. G. Read, E. Jefferys, and J. Luo. 1994. Diet of the Hastings River mouse (*Pseudomys oralis*). Wildlife Research 21:491–505.

Frankino, W. A., B. J. Zwaan, D. L. Stern, and P. M. Brakefield. 2005. Natural Selection and Developmental Constraints in the Evolution of Allometries. Science 307:718–720.

Fruciano, C. 2016. Measurement error in geometric morphometrics. Development Genes and Evolution 226:139–158.

Fruciano, C., M. A. Celik, K. Butler, T. Dooley, V. Weisbecker, and M. J. Phillips. 2017. Sharing is caring? Measurement error and the issues arising from combining 3D morphometric datasets. Ecology and Evolution 7:7034–7046.

Geffen, E., K. C. Rowe, and Y. Yom-Tov. 2011. Reproductive Rates in Australian Rodents Are Related to Phylogeny. PLOS One 6.

Guillerme, T., and V. Weisbecker. 2019. *landvR*: Tools for measuring landmark position variation. R package version 0.4.

Hautier, L., and P. G. Cox. 2015. Rodentia: a model order? Pages 1–18 *in* P. G. Cox and L. Hautier, eds. Evolution of the Rodents: Advances in Phylogeny, Functional Morphology and Development, Cambridge Studies in Morphology and Molecules: New Paradigms in Evolutionary Bio. Cambridge University Press, Cambridge.

Huxley, J. S., and G. Teissier. 1936. Terminology of Relative Growth. Nature 137:780.

Jamniczky, H. A., and B. Hallgrímsson. 2009. A comparison of covariance structure in wild and laboratory muroid crania. Evolution 63:1540–1556.

Jungers, W. L. 1982. Lucy's limbs: skeletal allometry and locomotion in *Australopithecus afarensis*. Nature 297:676.

Kimura, Y., M. T. R. Hawkins, M. M. McDonough, L. L. Jacobs, and L. J. Flynn. 2015. Corrected placement of *Mus-Rattus* fossil calibration forces precision in the molecular tree of rodents. Scientific Reports 5:14444.

Klingenberg, C. P. 2016. Size, shape, and form: concepts of allometry in geometric morphometrics. Development Genes and Evolution 226:113–137.

Lazzari, V., J. A. Schultz, P. Tafforeau, and T. Martin. 2010. Occlusal Pattern in Paulchoffatiid Multituberculates and the Evolution of Cusp Morphology in Mammaliamorphs with Rodent-like Dentitions. Journal of Mammalian Evolution 17:177–192.

Lillegraven, J. A. 1974. Biogeographical considerations of the marsupial-placental dichotomy. Annual Review of Ecology and Systematics 5:263–283.

Maestri, R., B. D. Patterson, R. Fornel, L. R. Monteiro, and T. R. O. de Freitas. 2016. Diet, bite force and skull morphology in the generalist rodent morphotype. Journal of Evolutionary Biology 29:2191–2204.

Marcy, A. E. 2018. 3D scans of Australian rodents - skull biodiversity. Project 561, MorphoSource. https://www.morphosource.org/Detail/ProjectDetail/Show/project_id/561.

Marcy, A. E., C. Fruciano, M. J. Phillips, K. Mardon, and V. Weisbecker. 2018. Low resolution scans can provide a sufficiently accurate, cost- and time-effective alternative to high resolution scans for 3D shape analyses. PeerJ 6:e5032.

Marcy, A. E., E. A. Hadly, E. Sherratt, K. Garland, and V. Weisbecker. 2016. Getting a head in hard soils: Convergent skull evolution and divergent allometric patterns explain shape variation in a highly diverse genus of pocket gophers (*Thomomys*). BMC Evolutionary Biology 16:207.

Marcy, A. E., T. Guillerme, E. Sherratt, K. C. Rowe, M. J. Phillips, V. Weisbecker. 2020. Data from: Australian rodents reveal conserved Craniofacial Evolutionary Allometry across 10 million years of murid evolution. American Naturalist, Dryad Digital Repository, https://doi.org/10.5061/dryad.z8w9ghx91.

Marroig, G., and J. Cheverud. 2010. Size as a line of least resistance II: direct selection on size or correlated response due to constraints? Evolution 64:1470–1488.

———. 2005. Size as a line of least evolutionary resistance: diet and adaptive morphological radiation in new world monkeys. Evolution 59:1128–1142.

Millar, J. S. 1977. Adaptive features of mammalian reproduction. Evolution 31:370–386.

Munds, R. A., R. H. Dunn, and G. E. Blomquist. 2018. Multivariate Craniodental Allometry of Tarsiers. International Journal of Primatology 39:252–268.

Murray, B. R., C. R. Dickman, C. H. S. Watts, and S. R. Morton. 1999. The dietary ecology of Australian desert rodents. Wildlife Research 26:421–437.

Paradis, E., and K. Schliep. 2018. *ape* 5.0: an environment for modern phylogenetics and evolutionary analyses in R. Bioinformatics 35:526–528.

Pélabon, C., C. Firmat, G. H. Bolstad, K. L. Voje, D. Houle, J. Cassara, A. L. Rouzic, et al. 2014. Evolution of morphological allometry. Annals of the New York Academy of Sciences 1320:58–75.

Polly, P. D. 2008. Adaptive Zones and the Pinniped Ankle: A Three-Dimensional Quantitative Analysis of Carnivoran Tarsal Evolution. Pages 167–196 *in* E. J. Sargis and M. Dagosto, eds. Mammalian Evolutionary Morphology: A Tribute to Frederick S. Szalay, Vertebrate Paleobiology and Paleoanthropology Series. Springer Netherlands, Dordrecht.

Polychronis, G., P. Christou, M. Mavragani, and D. J. Halazonetis. 2013. Geometric morphometric 3D shape analysis and covariation of human mandibular and maxillary first molars. American Journal of Physical Anthropology 152:186–196.

Porto, A., L. T. Shirai, F. B. de Oliveira, and G. Marroig. 2013. Size variation, growth strategies, and the evolution of modularity in the mammalian skull. Evolution 67:3305–3322.

R Core Team. 2019. R: A Language and Environment for Statistical Computing. R Foundation for Statistical Computing, Vienna, Austria.

Radinsky, L. B. 1985. Approaches in Evolutionary Morphology: A Search for Patterns. Annual Review of Ecology and Systematics 16:1–14.

Rambaut, A., and A. J. Drummond. 2007. Tracer v1.4: MCMC trace analyses tool.

Renaud, S., P. Chevret, and J. Michaux. 2007. Morphological vs. molecular evolution: ecology and phylogeny both shape the mandible of rodents. Zoologica Scripta 36:525–535.

Revell, L. J. 2012. *phytools*: an R package for phylogenetic comparative biology (and other things). Methods in Ecology and Evolution 3:217–223.

Rickart, E. A., D. S. Balete, R. M. Timm, P. A. Alviola, J. A. Esselstyn, and L. R. Heaney. 2019. Two new species of shrew-rats (*Rhynchomys*: Muridae: Rodentia) from Luzon Island, Philippines. Journal of Mammalogy 100:1112–1129.

Rohlf, F. J., and D. Slice. 1990. Extensions of the Procrustes Method for the Optimal Superimposition of Landmarks. Systematic Biology 39:40–59.

Rowe, K. C., A. S. Achmadi, and J. A. Esselstyn. 2016. Repeated evolution of carnivory among Indo-Australian rodents. Evolution 70:653–665.

Rowe, K. C., K. P. Aplin, P. R. Baverstock, and C. Moritz. 2011. Recent and Rapid Speciation with Limited Morphological Disparity in the Genus Rattus. Systematic Biology 60:188–203.

Rowe, K. C., M. L. Reno, D. M. Richmond, R. M. Adkins, and S. J. Steppan. 2008. Pliocene colonization and adaptive radiations in Australia and New Guinea (Sahul): Multilocus systematics of the old endemic rodents (Muroidea: Murinae). Molecular Phylogenetics and Evolution 47:84–101.

Ryan, S. A., K. E. Moseby, and D. C. Paton. 2003. Comparative foraging preferences of the greater stick-nest rat *Leporillus conditor* and the European rabbit *Oryctolagus cuniculus*: implications for regeneration of arid lands. Australian Mammalogy 25:135–146.

Schenk, J. J., K. C. Rowe, and S. J. Steppan. 2013. Ecological opportunity and incumbency in the diversification of repeated continental colonizations by muroid rodents. Systematic Biology 62:837–864.

Schluter, D. 1996. Adaptive radiation along genetic lines of least resistance. Evolution 50:1766–1774.

Schmidt, E. J., T. E. Parsons, H. A. Jamniczky, J. Gitelman, C. Trpkov, J. C. Boughner, C. C. Logan, et al. 2010. Micro-computed tomography-based phenotypic approaches in embryology: procedural artifacts on assessments of embryonic craniofacial growth and development. BMC Developmental Biology 10:18.

Serb, J. M., E. Sherratt, A. Alejandrino, and D. C. Adams. 2017. Phylogenetic convergence and multiple shell shape optima for gliding scallops (Bivalvia: Pectinidae). Journal of Evolutionary Biology 30:1736–1747.

Shirai, L. T., and G. Marroig. 2010. Skull modularity in neotropical marsupials and monkeys: size variation and evolutionary constraint and flexibility. Journal of Experimental Zoology Part B: Molecular and Developmental Evolution 314B:663–683.

Singleton, M. 2002. Patterns of cranial shape variation in the Papionini (Primates: Cercopithecinae). Journal of Human Evolution 42:547–578.

Smissen, P. J., and K. C. Rowe. 2018. Repeated biome transitions in the evolution of Australian rodents. Molecular Phylogenetics and Evolution 128:182–191.

Tamagnini, D., C. Meloro, and A. Cardini. 2017. Anyone with a Long-Face? Craniofacial Evolutionary Allometry (CREA) in a Family of Short-Faced Mammals, the Felidae. Evolutionary Biology 44:476–495.

Tsuboi, M., W. van der Bijl, B. T. Kopperud, J. Erritzøe, K. L. Voje, A. Kotrschal, K. E. Yopak, et al. 2018. Breakdown of brain–body allometry and the encephalization of birds and mammals. Nature Ecology & Evolution 2:1492–1500.

Venditti, C., A. Meade, and M. Pagel. 2011. Multiple routes to mammalian diversity. Nature 479:393–396.

Verde Arregoitia, L. D., D. O. Fisher, and M. Schweizer. 2017. Morphology captures diet and locomotor types in rodents. Royal Society Open Science 4:160957.

Voje, K. L., T. F. Hansen, C. K. Egset, G. H. Bolstad, and C. Pélabon. 2014. Allometric constraints and the evolution of allometry. Evolution 68:866–885.

Watts, C. H. S., and R. W. Braithwaite. 1978. The diet of *Rattus lutreolus* and five other rodents in southern Victoria. Wildlife Research 5:47–57.

Weisbecker, V., T. Guillerme, C. Speck, E. Sherratt, H. M. Abraha, A. C. Sharp, C. E. Terhune, et al. 2019. Individual variation of the masticatory system dominates 3D

skull shape in the herbivory-adapted marsupial wombats. Frontiers in Zoology 16:41.

Wilson, L. A. B., and M. R. Sánchez-Villagra. 2009. Diversity trends and their ontogenetic basis: an exploration of allometric disparity in rodents. Proceedings of the Royal Society B 277:1227–1234.

Wund, M. A., S. Valena, S. Wood, and J. A. Baker. 2012. Ancestral plasticity and allometry in threespine stickleback reveal phenotypes associated with derived, freshwater ecotypes. Biological Journal of the Linnean Society 105:573–583.

Yezerinac, S. M., S. C. Lougheed, and P. Handford. 1992. Measurement Error and Morphometric Studies: Statistical Power and Observer Experience. Systematic Biology 41:471–482.

Yoder, J. B., E. Clancey, S. Des Roches, J. M. Eastman, L. Gentry, W. Godsoe, T. J. Hagey, et al. 2010. Ecological opportunity and the origin of adaptive radiations. Journal of Evolutionary Biology 23:1581–1596.

Yom-Tov, Y. 1985. The reproductive rates of Australian rodents. Oecologia 66:250–255.

Zelditch, M. L., D. L. Swiderski, H. D. Sheets, and W. L. Fink. 2004. Geometric Morphometrics for Biologists. Elsevier, Amsterdam; Boston.

Tables

Table 1: Static allometry ANCOVA

	df	SS	MS	R^2	F	Z	Pr(>F)
Log(size)	1	0.625	0.625	0.365	450.	10.5	0.002
Species	37	0.694	0.019	0.405	13.5	19.9	0.002
Log(size):species	37	0.060	0.002	0.035	1.16	18.5	0.002
Residuals	241	0.335	0.001	0.195			
Total	316	1.713					

Static allometry (species-level) uses shapes and centroid sizes from all individuals from all 38 species. Abbreviations: degrees of freedom (df), sum of squares (SS), mean squares (MS), coefficient of determination (R^2), F-statistic (F), effect size (Z), and *p*-value estimated from parametric F-distributions (Pr(>F)).

Table 2: **Evolutionary allometry ANCOVA**

	df	SS	MS	R^2	F	Z	Pr(>F)
Log(size)	1	0.625	0.625	0.364	271	9.40	0.002
Clade	7	0.300	0.043	0.175	18.6	14.8	0.002
Log(size):Clade	7	0.096	0.014	0.056	5.94	10.8	0.002
Residuals	301	0.069	0.002	0.404			
Total	316	1.71					

Evolutionary allometry (among clades) uses the mean shapes and mean centroid sizes of the 37 species in the molecular phylogeny, which were then grouped into the eight clades (including the two monospecific lineages) indicated in figure 1. Abbreviations as in table 1.

Figure Legends

Figure 1: The time-calibrated molecular phylogeny generated for 37 of 38 species in this study. Node numbers correspond to those in figure 3. Filled nodes indicate the six major clades, whose ancestors are inferred to have each arrived in Australia at distinct times, after Aplin and Ford (2014). Species name colors were gradated across the genera in each major clade (e.g. blues for the Pseudomys division, node 12) and used consistently throughout. Phylogeny branches are tinted by body size (estimated from cranial centroid size (Zelditch et al. 2004)). These were generated by *phytools* (v.0.6-99) function *plotBranchbyTrait* using species mean cranial centroid sizes, estimated for ancestors from these tips (Revell 2012).

Figure 2: log centroid size, versus the regression scores of shape on size for each specimen (A). The overlaid grey line represents evolutionary allometry, or a regression on the mean specimen from every static allometry (Cheverud 1982) (see fig. 3). Predicted values for each species highlighting similarities in static allometric slopes (B).

Figure 3: Phylogenetic rarefaction: boxplot showing confidence intervals (95%, 50%) and median value (black point) for each clade after 100 rarefaction replicates (A). Median delta slope angle (°) is the difference between the observed and rarefied slopes. Each point gives the clade's median delta slope as compared to the 4.5° significant change in angle line (B). The x axis gives both the node number from figure 1 and the

number of species included in that node from figure 1; monospecific clades have only species abbreviation. Outliers are colored and identified in the legend.

Figure 4: Evolutionary allometric variation: plot of log centroid size versus the projected regression score of allometric shape on size (A). The grey regression line indicates the common evolutionary allometry trajectory. Labels and “hand-drawn” ellipses indicate species sharing a diet or locomotion specialization. PCA plot of PC1 and PC2 separates mean shapes of many specialists from the main cluster (B). Legend as in figure 2. Landmark heatmaps of shape change from the mean shape to PC1 minimum, dorsal view (C) and lateral view (D). Landmark heatmaps from mean shape to the PC1 maximum, dorsal view (E) and lateral view (F). Spheres show landmark positions for the mean shape and vectors show the direction of change to the extreme PC1 shapes.

Figure 1

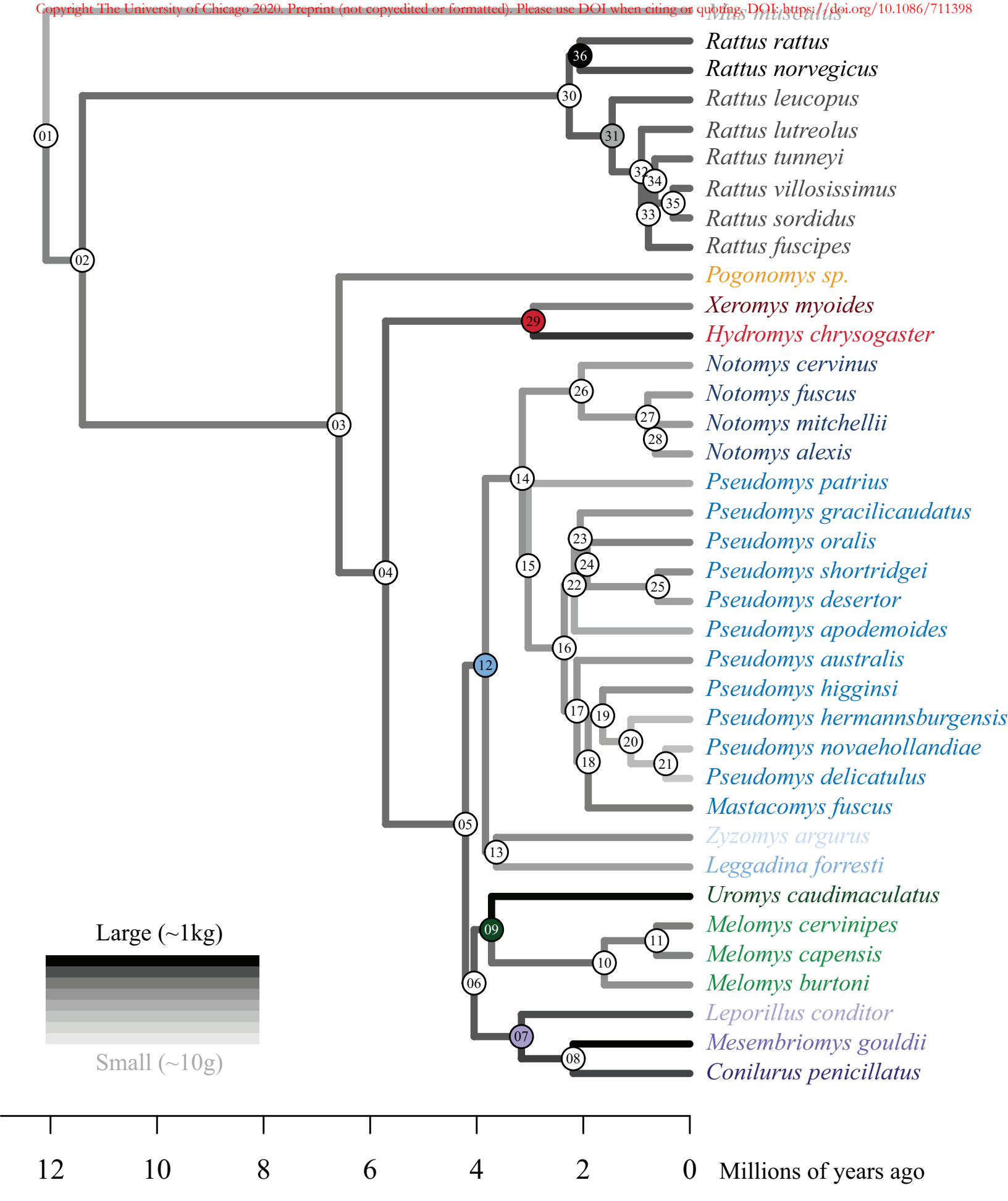

Figure 2

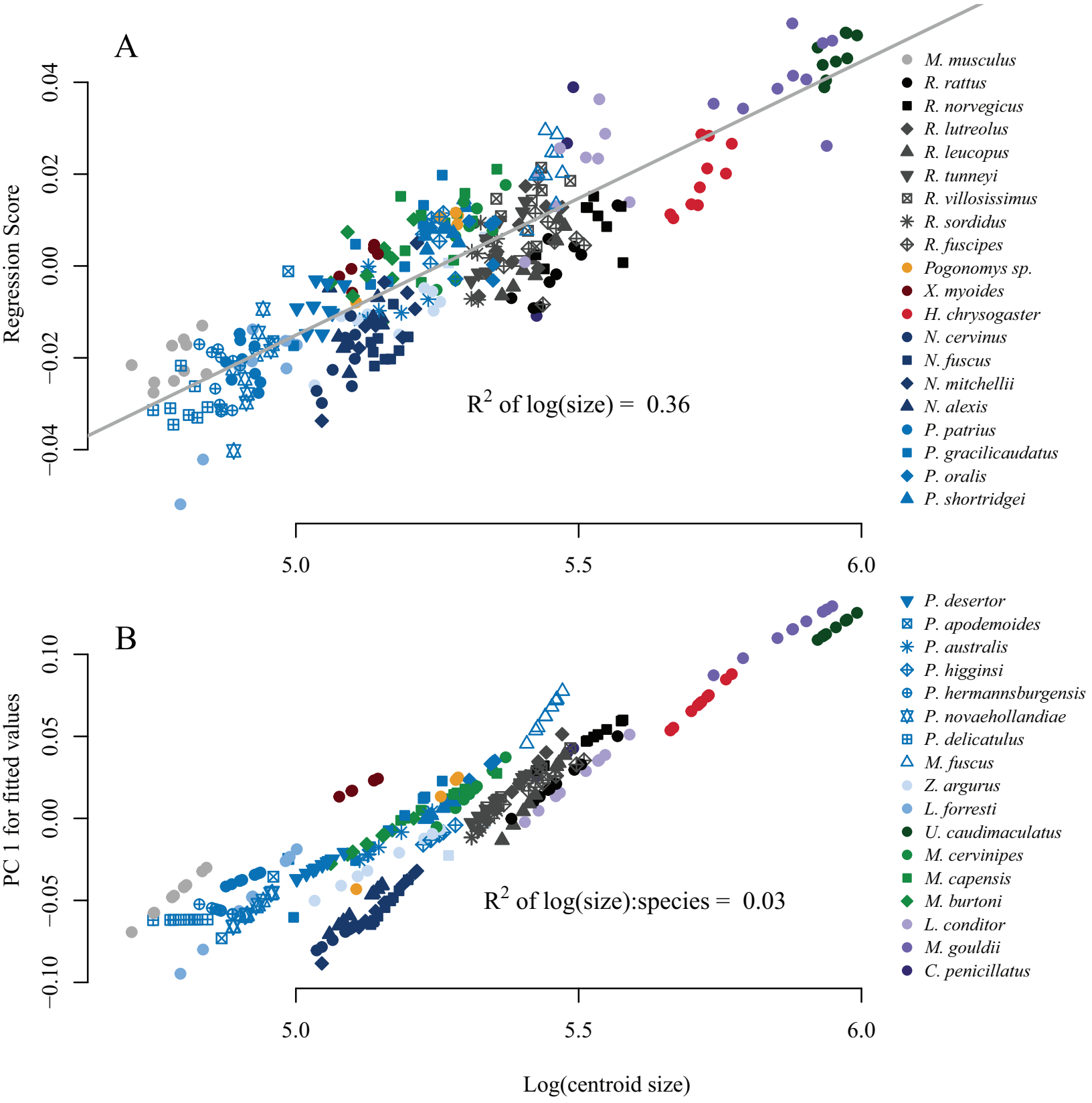

Figure 3

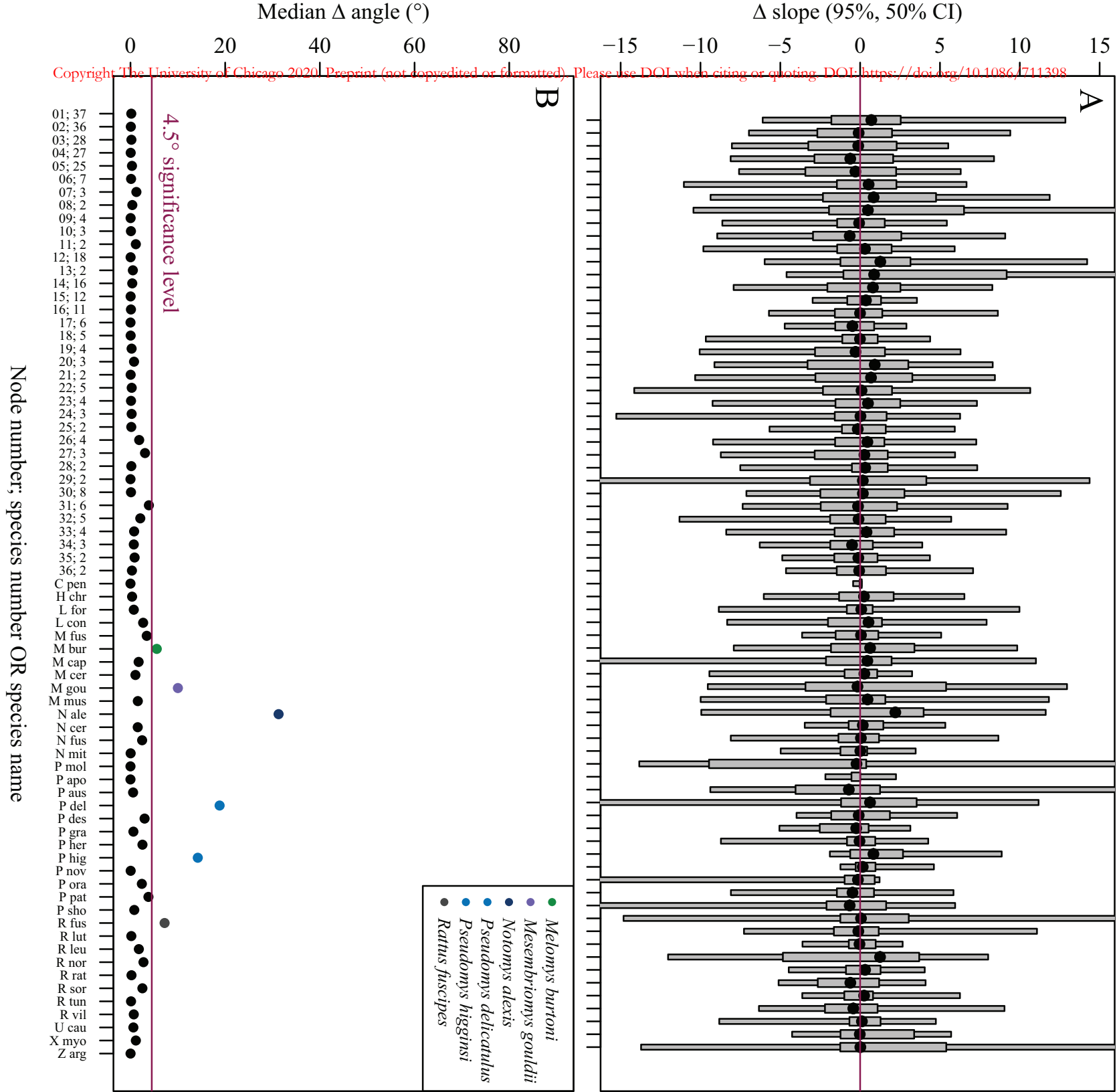

Figure 4

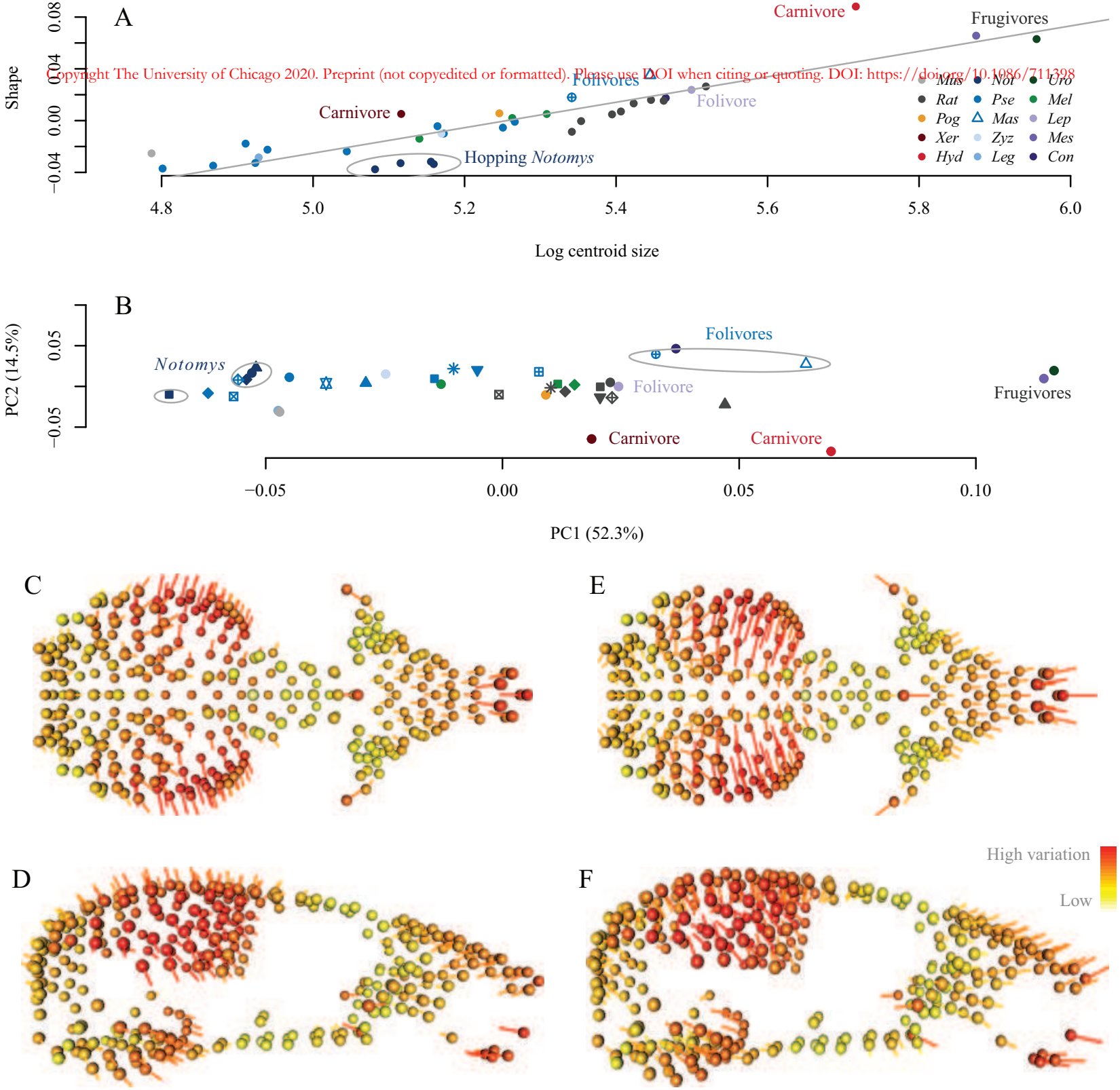

Australian rodents reveal conserved Cranial Evolutionary Allometry across 10 million years of murid evolution Ariel E. Marcy[1*], Thomas Guillerme[2], Emma Sherratt[3], Kevin C. Rowe[4,5], Matthew J. Phillips[6], and Vera Weisbecker[1,7]
[1]University of Queensland, School of Biological Sciences; University of Sheffield, Department of Animal and Plant Sciences; [3]University of Adelaide, School of Biological Sciences, [4]Museums Victoria, Sciences Department; [5]University of Melbourne, School of BioSciences; [6]Queensland University of Technology, School of Biology & Environmental Science; [7]Flinders University, College of Science and Engineering
*aemarcy@gmail.com **The American Naturalist**

Table S1: Specimen metadata

Museum	CatNum	Genus	Species	Sex
AM	M27465	Lep	con	Female
AM	S1600	Lep	con	Female
AM	M27463	Lep	con	Male
AM	M3061	Lep	con	Male
AM	M3063	Lep	con	Male
AM	M3065	Lep	con	Male
AM	S1597	Lep	con	Male
AM	M3409	Lep	con	Unknown
AM	M3457	Lep	con	Unknown
AM	M10765	Mas	fus	Female
AM	M7170	Mas	fus	Female
AM	M36984	Mas	fus	Male
AM	M27895	Mes	gou	Male
AM	M8345	Mes	gou	Male
AM	M27887	Not	ale	Female
AM	M5688	Not	ale	Female
AM	M10005	Not	ale	Male
AM	M23514	Not	cer	Female
AM	M8496	Not	cer	Female
AM	M23515	Not	cer	Male
AM	M23516	Not	cer	Male
AM	M8493	Not	cer	Male
AM	M8495	Not	cer	Male
AM	M8498	Not	cer	Male
AM	M23644	Not	fus	Female
AM	M23646	Not	fus	Female
AM	M23508	Not	fus	Male
AM	M4860	Not	fus	Male
AM	M4858	Not	mit	Female
AM	M4907	Not	mit	Female
AM	M5028	Not	mit	Female
AM	M8617	Not	mit	Female
AM	M3735	Not	mit	Male
AM	M4853	Not	mit	Male
AM	M8192	Not	mit	Male
AM	M10007	Pse	aus	Female

AM	M10008	Pse	aus	Female
AM	M10009	Pse	aus	Male
AM	M44869	Pse	aus	Male
AM	M9673	Pse	gra	Female
AM	M31106	Pse	gra	Male
AM	M9945	Pse	gra	Male
AM	M26079	Pse	her	Female
AM	M9207	Pse	her	Female
AM	M25376	Pse	her	Male
AM	M25377	Pse	her	Male
AM	M29421	Pse	her	Male
AM	M32487	Pse	her	Male
AM	M4872	Pse	hig	Female
AM	M4876	Pse	hig	Female
AM	M2468	Pse	hig	Female
AM	M4874	Pse	hig	Male
AM	M4875	Pse	hig	Male
AM	M4877	Pse	hig	Male
AM	M4878	Pse	hig	Male
AM	M12553	Pse	nov	Female
AM	M12557	Pse	nov	Female
AM	M25630	Pse	nov	Female
AM	M9155	Pse	nov	Female
AM	M12544	Pse	nov	Male
AM	M8938	Pse	nov	Male
AM	M9150	Pse	nov	Male
AM	M25633	Pse	ora	Female
AM	M29840	Pse	ora	Female
AM	M12346	Pse	ora	Male
AM	M6529	Xer	myo	Female
AM	M9991	Xer	myo	Female
AM	M10434	Xer	myo	Male
AM	M6868	Xer	myo	Male
AM	M21205	Zyz	arg	Female
AM	M21225	Zyz	arg	Male
AM	M24766	Zyz	arg	Male
MV	C31802	Mas	fus	Female
MV	C31804	Mas	fus	Female
MV	C31805	Mas	fus	Female
MV	C15025	Mas	fus	Male
MV	C15027	Mas	fus	Male
MV	C15034	Mas	fus	Male
MV	C25854	Mas	fus	Male

MV	DTC465	Mel	cap	Female
MV	DTC462	Mel	cap	Male
MV	DTC464	Mel	cap	Male
MV	DTC466	Mel	cap	Male
MV	C7570	Mes	gou	Female
MV	C7571	Mes	gou	Male
MV	C36854	Not	ale	Female
MV	C36848	Not	ale	Male
MV	C36885	Not	ale	Male
MV	C36886	Not	ale	Male
MV	C36892	Not	ale	Male
MV	C7356	Not	cer	Female
MV	C9081	Not	cer	Female
MV	C7833	Not	fus	Female
MV	C7834	Not	fus	Female
MV	C7835	Not	fus	Male
MV	C7836	Not	fus	Male
MV	C15045	Not	mit	Female
MV	C157	Pse	aus	Female
MV	C4886	Pse	aus	Male
MV	C4883	Pse	aus	Unknown
MV	C4884	Pse	aus	Unknown
MV	C10770	Pse	des	Female
MV	C36860	Pse	des	Female
MV	C36878	Pse	des	Female
MV	C10755	Pse	des	Male
MV	C36870	Pse	des	Male
MV	C36879	Pse	des	Male
MV	C18705	Pse	sho	Female
MV	C19922	Pse	sho	Female
MV	C22118	Pse	sho	Female
MV	C19925	Pse	sho	Male
MV	C19926	Pse	sho	Male
MV	C22111	Pse	sho	Male
MV	C37144	Pse	sho	Male
MV	C37172	Pse	sho	Male
MV	C20261	Rat	nor	Female
MV	C7338	Rat	nor	Female
MV	C29709	Rat	nor	Male
MV	C33155	Rat	nor	Male
MV	C6982	Uro	cau	Female
MV	C6983	Uro	cau	Female
MV	C6984	Uro	cau	Male

QM	J10055	Hyd	chr	Female
QM	J16824	Hyd	chr	Female
QM	J9835	Hyd	chr	Female
QM	J9944	Hyd	chr	Female
QM	J21273	Hyd	chr	Female
QM	J10127	Hyd	chr	Male
QM	J11137	Hyd	chr	Male
QM	J15330	Hyd	chr	Male
QM	J17593	Hyd	chr	Male
QM	J7889	Hyd	chr	Male
QM	JM11585	Leg	for	Female
QM	JM19648	Leg	for	Female
QM	JM3736	Leg	for	Female
QM	J14755	Leg	for	Male
QM	JM12328	Leg	for	Male
QM	JM10913	Leg	for	Unknown
QM	JM14441	Leg	for	Unknown
QM	JM14820	Leg	for	Unknown
QM	JM4955	Leg	for	Unknown
QM	J19997	Mel	bur	Female
QM	J4808	Mel	bur	Female
QM	J9801	Mel	bur	Female
QM	JM13946	Mel	bur	Female
QM	JM15015	Mel	bur	Female
QM	J10822	Mel	bur	Male
QM	J17693	Mel	bur	Male
QM	J9476	Mel	bur	Male
QM	JM1301	Mel	bur	Male
QM	JM3839	Mel	bur	Male
QM	JM13959	Mel	cap	Female
QM	JM13964	Mel	cap	Unknown
QM	JM4224	Mel	cap	Unknown
QM	JM4231	Mel	cap	Unknown
QM	JM4233	Mel	cap	Unknown
QM	JM4236	Mel	cap	Unknown
QM	J22537	Mel	cer	Female
QM	J3676	Mel	cer	Female
QM	J8956	Mel	cer	Female
QM	JM10991	Mel	cer	Female
QM	J22096	Mel	cer	Male
QM	J3675	Mel	cer	Male
QM	J6502	Mel	cer	Male
QM	J8960	Mel	cer	Male

QM	JM6185	Mel	cer	Male
QM	J19719	Mes	gou	Female
QM	J16976	Mes	gou	Male
QM	J19720	Mes	gou	Male
QM	JM20901	Mes	gou	Unknown
QM	J2562	Mes	gou	Unknown
QM	J3078	Mus	mus	Female
QM	J2993	Mus	mus	Female
QM	J16129	Mus	mus	Male
QM	J9161	Mus	mus	Male
QM	JM1272	Mus	mus	Male
QM	J13566	Mus	mus	Male
QM	J16141	Mus	mus	Male
QM	J16150	Mus	mus	Male
QM	J3105	Mus	mus	Unknown
QM	JM1027	Mus	mus	Unknown
QM	J14754	Not	ale	Male
QM	J10775	Not	fus	Male
QM	J3351	Not	mit	Male
QM	JM14683	Pog	sp.	Female
QM	JM10071	Pog	sp.	Male
QM	JM10590	Pog	sp.	Male
QM	JM8501	Pog	sp.	Male
QM	JM8841	Pog	sp.	Male
QM	JM11502	Pse	del	Female
QM	JM12690	Pse	del	Female
QM	JM12695	Pse	del	Female
QM	JM12708	Pse	del	Female
QM	JM18715	Pse	del	Female
QM	JM11350	Pse	del	Male
QM	JM19635	Pse	del	Male
QM	JM2133	Pse	del	Male
QM	JM8828	Pse	des	Female
QM	JM14592	Pse	des	Male
QM	JM4953	Pse	des	Male
QM	JM15791	Pse	gra	Female
QM	JM11213	Pse	gra	Male
QM	JM14420	Pse	gra	Male
QM	JM11182	Pse	gra	Male
QM	JM19872	Pse	gra	Unknown
QM	JM14849	Pse	gra	Unknown
QM	JM1289	Pse	her	Female
QM	JM2509	Pse	her	Female

QM	JM5019	Pse	her	Female
QM	J16683	Pse	her	Male
QM	JM14455	Pse	nov	Female
QM	J17920	Pse	nov	Male
QM	JM14454	Pse	nov	Male
QM	J20264	Pse	ora	Female
QM	JM13548	Pse	ora	Unknown
QM	JM13549	Pse	ora	Unknown
QM	JM11008	Pse	pat	Female
QM	JM11940	Pse	pat	Female
QM	JM8654	Pse	pat	Female
QM	JM10864	Pse	pat	Male
QM	JM10865	Pse	pat	Male
QM	JM12674	Pse	pat	Male
QM	JM8830	Pse	pat	Male
QM	JM12363	Pse	pat	Male
QM	JM15010	Pse	pat	Unknown
QM	J3488	Pse	sho	Male
QM	J11226	Rat	fus	Female
QM	J12672	Rat	fus	Female
QM	J19105	Rat	fus	Female
QM	JM12469	Rat	fus	Female
QM	J10939	Rat	fus	Male
QM	J3681	Rat	fus	Male
QM	J9687	Rat	fus	Male
QM	JM11916	Rat	fus	Male
QM	JM15739	Rat	fus	Male
QM	J10136	Rat	leu	Female
QM	J8280	Rat	leu	Female
QM	JM172014	Rat	leu	Female
QM	JM2127	Rat	leu	Female
QM	J10139	Rat	leu	Male
QM	J10197	Rat	leu	Male
QM	JM11803	Rat	leu	Male
QM	JM17301	Rat	leu	Male
QM	JM1768	Rat	leu	Male
QM	J16918	Rat	lut	Female
QM	J22555	Rat	lut	Female
QM	J22595	Rat	lut	Female
QM	J8922	Rat	lut	Female
QM	J20340	Rat	lut	Male
QM	J22819	Rat	lut	Male
QM	J22885	Rat	lut	Male

QM	JM14757	Rat	lut	Male
QM	J22598	Rat	lut	Male
QM	J11439	Rat	nor	Female
QM	J17925	Rat	nor	Female
QM	J10052	Rat	nor	Male
QM	J17540	Rat	nor	Male
QM	J17927	Rat	nor	Male
QM	J10961	Rat	rat	Female
QM	J20163	Rat	rat	Female
QM	J3326	Rat	rat	Female
QM	J4085	Rat	rat	Female
QM	J16172	Rat	rat	Male
QM	J17793	Rat	rat	Male
QM	J17798	Rat	rat	Male
QM	J17923	Rat	rat	Male
QM	J6275	Rat	rat	Male
QM	J17959	Rat	sor	Female
QM	J22871	Rat	sor	Female
QM	J3836	Rat	sor	Female
QM	J8929	Rat	sor	Female
QM	J17955	Rat	sor	Male
QM	J20409	Rat	sor	Male
QM	J9172	Rat	sor	Male
QM	JM1313	Rat	sor	Male
QM	JM9078	Rat	sor	Male
QM	J16895	Rat	tun	Female
QM	J22604	Rat	tun	Female
QM	J9206	Rat	tun	Female
QM	J9786	Rat	tun	Female
QM	J22095	Rat	tun	Male
QM	J22099	Rat	tun	Male
QM	J9566	Rat	tun	Male
QM	J9571	Rat	tun	Male
QM	JM12504	Rat	tun	Male
QM	J16963	Rat	vil	Female
QM	J16964	Rat	vil	Female
QM	J20160	Rat	vil	Female
QM	J22613	Rat	vil	Female
QM	J9162	Rat	vil	Female
QM	J16967	Rat	vil	Male
QM	J19057	Rat	vil	Male
QM	J6719	Rat	vil	Male
QM	J6721	Rat	vil	Male

QM	J9682	Rat	vil	Male
QM	J22538	Uro	cau	Female
QM	JM2344	Uro	cau	Female
QM	J22607	Uro	cau	Female
QM	J11512	Uro	cau	Male
QM	J20347	Uro	cau	Male
QM	J9304	Uro	cau	Male
QM	JM4924	Xer	myo	Female
QM	JM2708	Xer	myo	Male
QM	J22399	Zyz	arg	Female
QM	JM12723	Zyz	arg	Female
QM	J22398	Zyz	arg	Male
QM	J22401	Zyz	arg	Male
QM	JM14576	Zyz	arg	Unknown
QM	JM14578	Zyz	arg	Unknown
SAM	M1796	Con	pen	Male
SAM	M4071	Con	pen	Male
SAM	M392	Con	pen	Unknown
SAM	M11646	Pse	apo	Female
SAM	M13666	Pse	apo	Male
SAM	M3468	Pse	apo	Unknown
SAM	M4379	Zyz	ped	Female
SAM	M2412	Zyz	ped	Unknown

Museum abbreviations are as follows: Australian Museum (AM), Museums Victoria (MV), Queensland Museum (QM), and South Australian Museum (SAM). Genus and species names given with three letter abbreviations and can be identified in figure 1.

Table S2: Landmark definitions

Name	Definition	Points included
LM1	Anterior most point of nasal along central suture	1
LM2	Central intersection of nasal and frontal bones	1
LM3	Central intersection of frontal and parietal	1
LM4	Central intersection of parietal and interparietal	1
LM5	Central intersection interparietal and occipital	1
LM6	Dorsal and central most point of the foramen magnum	1
LM7	Ventral and central most point of the foramen magnum	1
LM8	Central intersection of basioccipital & basisphenoid suture	1
LM9	Central and posterior most point of palatine	1
LM10	Center point btwn posterior most tips of anterior palatine foramen	1
LM11	Center point btwn anterior most tips of anterior palatine foramen	1
LM12	Posterior point of incisor alveolar margin with center of incisor (r)	1
LM13	Posterior point of incisor alveolar margin with center of incisor (l)	1
LM14	Anterior-ventral most pt of intersection btwn premaxilla & incisor (r)	1
LM15	Anterior-ventral most pt of intersection btwn premaxilla & incisor (l)	1
LM16	Anterior & lateral most point of premaxillary/nasal suture (r)	1

LM17	Anterior & lateral most point of premaxillary/nasal suture (l)	1
LM18	Anterior most point of the infraorbital foramen (right)	1
LM19	Anterior most point of the infraorbital foramen (left)	1
LM20	Lateral edge of infraorbital foramen and anterior tip of zygomatic (r)	1
LM21	Lateral edge of infraorbital foramen and anterior tip of zygomatic (l)	1
LM22	Most posterior point of supraorbital (right)	1
LM23	Most posterior point of supraorbital (left)	1
LM24	Posterior intersection of the premaxilla and maxilla (right)	1
LM25	Posterior intersection of the premaxilla and maxilla (left)	1
LM26	Intersection of the frontal, squamosal, and parietal bones (r)	1
LM27	Intersection of the frontal, squamosal, and parietal bones (l)	1
LM28	Anterior pt of intersection of posterior zygomatic with squamosal (r)	1
LM29	Anterior pt of intersection of posterior zygomatic with squamosal (l)	1
LM30	Posterior most point of intersection of zygomatic with squamosal (r)	1
LM31	Posterior most point of intersection of zygomatic with squamosal (l)	1
LM32	Intersection of parietal, squamosal, and occipital sutures (r)	1
LM33	Intersection of parietal, squamosal, and occipital sutures (l)	1
LM34	Intersection of parietal and occipital bones (right)	1
LM35	Intersection of parietal and occipital bones (left)	1
LM36	Lateral occipital condyle intersect with edge of foramen magnum (r)	1
LM37	Lateral occipital condyle intersect with edge of foramen magnum (l)	1
LM38	Paraoccipital process (right)	1
LM39	Paraoccipital process (left)	1
LM40	Lingual tip of bulla (right)	1
LM41	Lingual tip of bulla (left)	1
LM42	Posterior point of pterygoid process (right)	1
LM43	Posterior point of pterygoid process (left)	1
LM44	Posterior most point of tooth row (right)	1
LM45	Posterior most point of tooth row (left)	1
LM46	Anterior most point of tooth row (right)	1
LM47	Anterior most point of tooth row (left)	1
LM48	Posterior most point of maxilla part of zygomatic arch (right)	1
LM49	Posterior most point of maxilla part of zygomatic arch (left)	1
LM50	Posterior point of external auditory meatus (right)	1
LM51	Posterior point of external auditory meatus (left)	1
LM52	Dorsal most point of external auditory meatus (right)	1
LM53	Dorsal most point of external auditory meatus (left)	1
LM54	Anterior & ventral most point of external auditory meatus (r)	1
LM55	Anterior & ventral most point of external auditory meatus (l)	1
LM56	Posterior-dorsal most pt of intersection of dentary & squamosal (r)	1
LM57	Posterior-dorsal most pt of intersection of dentary & squamosal (l)	1
LM58	Anterior and lateral most point of the zygomatic arch (right)	1
LM59	Anterior and lateral most point of the zygomatic arch (left)	1
LM60	Central anterior ventral most point of nasal opening	1
Curve1	Central nasal suture between LM1 and 2	3
Curve2	Central frontal suture between LM2 and 3	4
Curve3	Central parietal suture between LM3 and 4	2
Curve4	Central interparietal line between LM4 and 5	1

Curve5	Central occipital line between LM5 and 6	2
Curve6	Central basisphenoid suture between LM7 and 8	2
Curve7	Central line of hard palate between LM9 and 10	3
Curve8	Nasal and premaxilla suture between LM16 and 2 (right)	5
Curve9	Nasal and premaxilla suture between LM15 and 2 (left)	5
Curve10	Lateral most edge of frontal between LM2 and 26 (right)	3
Curve11	Lateral most edge of frontal between LM2 and 27 (left)	3
Curve12	Frontal and parietal suture between LM3 and 26 (right)	3
Curve13	Frontal and parietal suture between LM3 and 27 (left)	3
Curve14	Parietal and squamosal suture between LM26 and 32 (r)	6
Curve15	Parietal and squamosal suture between LM27 and 33 (l)	6
Curve16	Parietal and interparietal suture between LM34 and 4 (right)	2
Curve17	Parietal and interparietal suture between LM35 and 4 (left)	2
Curve18	Interparietal and occipital suture between LM34 and 5 (r)	3
Curve19	Interparietal and occipital suture between LM35 and 5 (l)	3
Curve20	Lateral most edge of occipital between LM34 and 36 (right)	3
Curve21	Lateral most edge of occipital between LM35 and 37 (left)	3
Curve22	Dorsal-posterior most edge of foramen magnum btwn LM6 & 36 (r)	2
Curve23	Dorsal-posterior most edge of foramen magnum btwn LM6 & 37 (l)	2
Curve24	Ventral-posterior most edge of foramen magnum btwn LM36 & 7 (r)	3
Curve25	Ventral-posterior most edge of foramen magnum btwn LM37 & 7 (l)	3
Curve26	Posterior outline of auditory bulla between LM38 & LM40 (r)	5
Curve27	Posterior outline of auditory bulla between LM39 & LM41 (l)	5
Curve28	Anterior outline of auditory bulla between LM40 & LM54 (r)	3
Curve29	Anterior outline of auditory bulla between LM41 & LM55 (l)	3
Curve30	Ventral surface of pterygoid between LM42 and LM 44 (r)	2
Curve31	Ventral surface of pterygoid between LM43 and LM 45 (left)	2
Curve32	Lingual edge of tooth row between LM44 and 46 (right)	3
Curve33	Lingual edge of tooth row between LM45 and 47 (left)	3
Curve34	Posterior most edge of maxilla between LM46 and 48 (right)	3
Curve35	Posterior most edge of maxilla between LM47 and 49 (left)	3
Curve36	Lateral most edge of maxilla between LM48 and 20 (right)	2
Curve37	Lateral most edge of maxilla between LM49 and 21 (left)	2
Curve38	Anterior edge of lateral supraorbital between LM58 & 20 (r)	2
Curve39	Anterior edge of lateral supraorbital between LM59 & 21 (l)	2
Curve40	Lateral and anterior edge of orbit between LM20 and 22 (r)	1
Curve41	Lateral and anterior edge of orbit between LM21 and 23 (l)	1
Curve42	Medial edge of supraorbital between LM22 and 18 (right)	3
Curve43	Medial edge of supraorbital between LM22 and 18 (left)	3
Curve44	Incisor root and ventral supraorbital between LM18 & 58 (r)	3
Curve45	Incisor root and ventral supraorbital between LM19 & 59 (l)	3
Curve46	Anterior edge of squamosal between LM26 and 28 (right)	3
Curve47	Anterior edge of squamosal between LM27 and 29 (left)	3
Curve48	Intersection of squamosal with zygomatic between LM28 & 30 (r)	2
Curve49	Intersection of squamosal with zygomatic between LM29 and 31 (l)	2
Patch1	Nasal surface between Curve1 and Curve 8 (right)	5
Patch2	Nasal surface between Curve1 and Curve9 (left)	5
Patch3	Frontal surface between Curve2, Curve 10, and Curve12 (r)	7

Patch4	Frontal surface between Curve2, Curve 11, and Curve13 (l)	7
Patch5	Parietal surface btwn Curve3, Curve12, Curve14, and 16 (r)	14
Patch6	Parietal surface between Curve3, Curve13, 15 and 17 (left)	14
Patch7	Interparietal surface btwn Curve4, Curve16, & Curve18 (r)	3
Patch8	Interparietal surface btwn Curve4, Curve17, and Curve19 (l)	3
Patch9	Occipital surface btwn Curves5, 16, 20, & 22 (r)	8
Patch10	Occipital surface between Curves5, 17, 21, & Curve23 (l)	8
Patch11	Maxillary surface between Curve34, Curve36, & Curve38 (r)	8
Patch12	Maxillary surface between Curve35, Curve37 & Curve39 (l)	8
Patch13	Auditory bullae between Curve28 and 30 (right)	10
Patch14	Auditory bullae between Curve29 and 31 (left)	10
Patch15	Squamosal surface between Curve14 and 48 (right)	7
Patch16	Squamosal surface between Curve15 and 49 (left)	7

Landmark types are as follows: fixed landmark (LM, n = 60), curve semi-landmark (curve, n = 141), and patch semi-landmarks (patch, n = 124). 325 landmarks in total. Definitions and LM numbers can be matched to those depicted in figure S1.

Table S3: GenBank accession numbers for species in phylogeny

Taxon	Voucher	Voucher Institution
Apodemus agrarius	MVZ 159220	Museum of Vertebrate Zoology
Apodemus draco	Unknown	Unknown
Apodemus flavicollis	MVZ 181468	Museum of Vertebrate Zoology
Apodemus gurkha	HS 1317	Hitoshi Suszuki, Hokkaido University
Apodemus mystacinus	CMNH SP7861	Carnegie Museum of Natural History
Apodemus semotus	MVZ 180489	Museum of Vertebrate Zoology
Apodemus speciosus	HS 240	Hitoshi Suszuki, Hokkaido University
Apodemus sylvaticus	HS 1290	Hitoshi Suszuki, Hokkaido University
Conilurus penicillatus	ABTC 7411	South Australian Museum
Grammomys ibeanus	FMNH 151232	Field Museum of Natural History
Hydromys chrysogaster	ABTC 45619/KUMNH 160729/KUMNH 160730	South Australian Museum/Univ. Kansas Museum of Natural History
Leggadina forresti	ABTC 36085	South Australian Museum
Leggadina lakedownensis	ABTC 07406	South Australian Museum
Leopoldamys sabanus	CMNH 102138	Carnegie Museum of Natural History
Leporillus conditor	ABTC 13335	South Australian Museum
Mastacomys fuscus	ABTC 07354	South Australian Museum
Melomys bannisteri	M42669	Western Australian Museum
Melomys cooperae	M43822	Western Australian Museum
Melomys rufescens	ABTC 43071	South Australian Museum
Melomys burtoni	CACG I40	Centre for Animal Conservation Genetics, Southern Cross University
Melomys capensis	M11443	South Australian Museum
Melomys cervinipes	ABTC 08336	South Australian Museum
Mesembriomys gouldii	ABTC 07412	South Australian Museum

Mus cookii	USNM 583802	United States National Museum
Mus mattheyi	HS 865	Hitoshi Suszuki, Hokkaido University
Mus musculus	strain C57BL/6J GRCm38.p4 Genome Asssembly	na
Mus pahari	AMCC 110800	American Museum of Natural History
Mus platythrix	HS 628	Hitoshi Suszuki, Hokkaido University
Notomys alexis	ABTC 61767	South Australian Museum
Notomys aquilo	ABTC 18252	South Australian Museum
Notomys cervinus	ABTC 27130	South Australian Museum
Notomys fuscus	ABTC 117695	South Australian Museum
Notomys mitchellii	ABTC 07351	South Australian Museum
Oenomys hypoxanthus	CMNH 102549/CMNH 102548	Carnegie Museum of Natural History
Parotomys brantsii	H656	na
Paruromys dominator	ABTC 65763	South Australian Museum
Pogonomys loriae	KUMNH 160668	University of Kansas Museum of Natural History
Praomys jacksoni	CMNH 102583/CMNH 102584	Carnegie Museum of Natural History
Pseudomys albocinereus	ABTC 08044	South Australian Museum
Pseudomys apodemoides	Z7296	Museums Victoria
Pseudomys australis	ABTC 35951	South Australian Museum
Pseudomys bolami	ABTC 08065	South Australian Museum
Pseudomys chapmani	ABTC 62178	South Australian Museum
Pseudomys delicatulus	ABTC 62035	South Australian Museum
Pseudomys desertor	Z21274	Museums Victoria
Pseudomys fieldi	ABTC 08164	South Australian Museum
Pseudomys fumeus	Z25963	Museums Victoria
Pseudomys gracilicaudatus	ABTC 08031	South Australian Museum
Pseudomys hermannsburgensis	ABTC 91375	South Australian Museum
Pseudomys higginsi	ABTC 08139	South Australian Museum
Pseudomys johnsoni	ABTC 08055	South Australian Museum
Pseudomys nanus	ABTC 08056	South Australian Museum
Pseudomys novaehollandiae	ABTC 08140	South Australian Museum
Pseudomys occidentalis	ABTC 08042	South Australian Museum
Pseudomys oralis	KR033	Centre for Animal Conservation Genetics, Southern Cross University
Pseudomys patrius	ABTC 32205	South Australian Museum
Pseudomys shortridgei	ABTC 08079	South Australian Museum

Rattus leucopus	ABTC 160770	South Australian Museum
Rattus fuscipes	CACG C21	Centre for Animal Conservation Genetics, Southern Cross University
Rattus lutreolus	Z25082	Museums Victoria
Rattus norvegicus	Rnor_6.0 reference Annotation Release 106	na
Rattus rattus	T820/T660/CACG A65	Centre for Animal Conservation Genetics, Southern Cross University
Rattus sordidus	CACG RAT91	Centre for Animal Conservation Genetics, Southern Cross University
Rattus tunneyi	CACG RAT132	Centre for Animal Conservation Genetics, Southern Cross University
Rattus villosissimus	ABTC 00549	South Australian Museum
Rhabdomys pumilio	RA 23	Ronald Adkins
Tokudaia osimensis	HS1162	Hitoshi Suszuki, Hokkaido University
Uromys caudimaculatus	MVZ 193100	Museum of Vertebrate Zoology
Xeromys myoides	ABTC 30709	South Australian Museum
Zyzomys argurus	ABTC 07908	South Australian Museum
Zyzomys maini	ABTC 08025	South Australian Museum
Zyzomys palatalis	ABTC 30744	South Australian Museum
Zyzomys woodwardi	ABTC 07092	South Australian Museum

Table S4: Homogenity of slope test

	C_pen	H_chr	L_con	L_for	M_bur	M_cap	M_cer	M_fus	M_gou
C_pen	1	0.192	0.172	0.375	0.679	0.511	0.551	0.551	0.224
H_chr	0.192	1	0.022	0.03	0.098	0.036	0.04	0.315	0.11
L_con	0.172	0.022	1	0.094	0.244	0.05	0.02	0.333	0.028
L_for	0.375	0.03	0.094	1	0.064	0.07	0.082	0.068	0.194
M_bur	0.679	0.098	0.244	0.064	1	0.285	0.493	0.21	0.347
M_cap	0.511	0.036	0.05	0.07	0.285	1	0.964	0.463	0.633
M_cer	0.551	0.04	0.02	0.082	0.493	0.964	1	0.459	0.431
M_fus	0.551	0.315	0.333	0.068	0.21	0.463	0.459	1	0.776
M_gou	0.224	0.11	0.028	0.194	0.347	0.633	0.431	0.776	1
M_mus	0.307	0.072	0.026	0.092	0.024	0.032	0.072	0.012	0.098
N_ale	0.629	0.152	0.016	0.439	0.623	0.305	0.261	0.487	0.148
N_cer	0.204	0.046	0.04	0.076	0.12	0.132	0.072	0.192	0.152
N_fus	0.469	0.244	0.16	0.277	0.383	0.058	0.088	0.086	0.062
N_mit	0.447	0.112	0.144	0.253	0.914	0.856	0.76	0.681	0.291
P_apo	0.19	0.014	0.03	0.232	0.064	0.052	0.028	0.024	0.224
P_aus	0.493	0.162	0.168	0.058	0.457	0.691	0.747	0.186	0.487
P_del	0.359	0.291	0.521	0.044	0.158	0.136	0.255	0.202	0.152
P_des	0.822	0.373	0.277	0.12	0.651	0.737	0.653	0.679	0.884
P_gra	0.549	0.114	0.026	0.19	0.749	0.283	0.359	0.144	0.525
P_her	0.417	0.182	0.194	0.006	0.114	0.184	0.206	0.202	0.439
P_hig	0.569	0.06	0.044	0.18	0.599	0.331	0.19	0.75	0.246

P_sp.	0.461	0.024	0.066	0.248	0.529	0.719	0.671	0.311	0.457
P_nov	0.084	0.01	0.04	0.01	0.01	0.014	0.024	0.042	0.291
P_ora	0.569	0.086	0.094	0.255	0.852	0.543	0.409	0.299	0.437
P_pat	0.749	0.445	0.198	0.084	0.375	0.236	0.22	0.23	0.455
P_sho	0.529	0.064	0.042	0.236	0.643	0.98	0.982	0.333	0.375
R_fus	0.479	0.048	0.188	0.303	0.731	0.976	0.996	0.615	0.224
R_leu	0.483	0.092	0.098	0.008	0.192	0.138	0.118	0.425	0.246
R_lut	0.633	0.026	0.058	0.024	0.78	0.421	0.339	0.677	0.309
R_nor	0.619	0.022	0.128	0.585	0.988	0.998	0.976	0.758	0.116
R_rat	0.749	0.078	0.257	0.172	0.852	0.814	0.77	0.699	0.096
R_sor	0.541	0.046	0.07	0.042	0.912	0.585	0.481	0.575	0.186
R_tun	0.561	0.078	0.08	0.124	0.82	0.164	0.062	0.375	0.152
R_vil	0.467	0.044	0.13	0.086	0.938	0.263	0.285	0.212	0.118
U_cau	0.84	0.888	0.93	0.8	0.946	0.908	0.906	0.842	0.856
X_myo	0.238	0.277	0.176	0.01	0.076	0.078	0.072	0.046	0.437
Z_arg	0.752	0.086	0.046	0.02	0.341	0.75	0.888	0.331	0.621
Z_ped	0.487	0.034	0.216	0.182	0.697	0.836	0.89	0.363	0.208

	M_gou	**M_mus**	**N_ale**	**N_cer**	**N_fus**	**N_mit**	**P_apo**	**P_aus**	**P_del**
C_pen	0.224	0.307	0.629	0.204	0.469	0.447	0.19	0.493	0.359
H_chr	0.11	0.072	0.152	0.046	0.244	0.112	0.014	0.162	0.291
L_con	0.028	0.026	0.016	0.04	0.16	0.144	0.03	0.168	0.521
L_for	0.194	0.092	0.439	0.076	0.277	0.253	0.232	0.058	0.044
M_bur	0.347	0.024	0.623	0.12	0.383	0.914	0.064	0.457	0.158
M_cap	0.633	0.032	0.305	0.132	0.058	0.856	0.052	0.691	0.136
M_cer	0.431	0.072	0.261	0.072	0.088	0.76	0.028	0.747	0.255
M_fus	0.776	0.012	0.487	0.192	0.086	0.681	0.024	0.186	0.202
M_gou	1	0.098	0.148	0.152	0.062	0.291	0.224	0.487	0.152
M_mus	0.098	1	0.158	0.012	0.2	0.088	0.032	0.064	0.062
N_ale	0.148	0.158	1	0.248	0.05	0.449	0.2	0.22	0.224
N_cer	0.152	0.012	0.248	1	0.03	0.202	0.176	0.058	0.22
N_fus	0.062	0.2	0.05	0.03	1	0.024	0.03	0.297	0.355
N_mit	0.291	0.088	0.449	0.202	0.024	1	0.172	0.259	0.24
P_apo	0.224	0.032	0.2	0.176	0.03	0.172	1	0.022	0.01
P_aus	0.487	0.064	0.22	0.058	0.297	0.259	0.022	1	0.09
P_del	0.152	0.062	0.224	0.22	0.355	0.24	0.01	0.09	1
P_des	0.884	0.022	0.697	0.669	0.481	0.667	0.186	0.503	0.08
P_gra	0.525	0.088	0.517	0.084	0.214	0.778	0.122	0.042	0.118
P_her	0.439	0.052	0.13	0.088	0.084	0.158	0.02	0.118	0.058
P_hig	0.246	0.066	0.25	0.112	0.068	0.617	0.05	0.337	0.234
P_sp.	0.457	0.06	0.178	0.068	0.493	0.629	0.022	0.914	0.257
P_nov	0.291	0.014	0.008	0.004	0.016	0.06	0.13	0.004	0.002
P_ora	0.437	0.08	0.489	0.068	0.06	0.597	0.158	0.202	0.126

P_pat	0.455	0.098	0.469	0.379	0.443	0.321	0.24	0.313	0.018
P_sho	0.375	0.056	0.367	0.06	0.06	0.936	0.088	0.541	0.2
R_fus	0.224	0.204	0.281	0.04	0.056	0.737	0.056	0.952	0.343
R_leu	0.246	0.062	0.032	0.052	0.034	0.104	0.018	0.176	0.349
R_lut	0.309	0.024	0.146	0.106	0.05	0.579	0.054	0.218	0.325
R_nor	0.116	0.138	0.938	0.09	0.236	0.98	0.2	0.996	0.363
R_rat	0.096	0.144	0.523	0.138	0.467	0.75	0.032	0.93	0.541
R_sor	0.186	0.028	0.265	0.118	0.305	0.651	0.048	0.643	0.373
R_tun	0.152	0.032	0.397	0.072	0.355	0.271	0.058	0.393	0.297
R_vil	0.118	0.052	0.144	0.032	0.663	0.355	0.038	0.691	0.403
U_cau	0.856	0.653	0.886	0.822	0.966	0.866	0.601	0.952	0.78
X_myo	0.437	0.008	0.136	0.232	0.792	0.124	0.022	0.096	0.038
Z_arg	0.621	0.1	0.222	0.076	0.014	0.563	0.042	0.138	0.148
Z_ped	0.208	0.192	0.138	0.09	0.082	0.766	0.032	0.423	0.467

	P_des	P_gra	P_her	P_hig	P_sp.	P_nov	P_ora	P_pat	P_sho	R_fus
C_pen	0.822	0.549	0.417	0.569	0.461	0.084	0.569	0.749	0.529	0.479
H_chr	0.373	0.114	0.182	0.06	0.024	0.01	0.086	0.445	0.064	0.048
L_con	0.277	0.026	0.194	0.044	0.066	0.04	0.094	0.198	0.042	0.188
L_for	0.12	0.19	0.006	0.18	0.248	0.01	0.255	0.084	0.236	0.303
M_bur	0.651	0.749	0.114	0.599	0.529	0.01	0.852	0.375	0.643	0.731
M_cap	0.737	0.283	0.184	0.331	0.719	0.014	0.543	0.236	0.98	0.976
M_cer	0.653	0.359	0.206	0.19	0.671	0.024	0.409	0.22	0.982	0.996
M_fus	0.679	0.144	0.202	0.75	0.311	0.042	0.299	0.23	0.333	0.615
M_gou	0.884	0.525	0.439	0.246	0.457	0.291	0.437	0.455	0.375	0.224
M_mus	0.022	0.088	0.052	0.066	0.06	0.014	0.08	0.098	0.056	0.204
N_ale	0.697	0.517	0.13	0.25	0.178	0.008	0.489	0.469	0.367	0.281
N_cer	0.669	0.084	0.088	0.112	0.068	0.004	0.068	0.379	0.06	0.04
N_fus	0.481	0.214	0.084	0.068	0.493	0.016	0.06	0.443	0.06	0.056
N_mit	0.667	0.778	0.158	0.617	0.629	0.06	0.597	0.321	0.936	0.737
P_apo	0.186	0.122	0.02	0.05	0.022	0.13	0.158	0.24	0.088	0.056
P_aus	0.503	0.042	0.118	0.337	0.914	0.004	0.202	0.313	0.541	0.952
P_del	0.08	0.118	0.058	0.234	0.257	0.002	0.126	0.018	0.2	0.343
P_des	1	0.774	0.168	0.595	0.633	0.068	0.657	0.842	0.603	0.575
P_gra	0.774	1	0.082	0.311	0.545	0.022	0.824	0.429	0.627	0.619
P_her	0.168	0.082	1	0.222	0.128	0.016	0.15	0.146	0.14	0.287
P_hig	0.595	0.311	0.222	1	0.096	0.068	0.806	0.329	0.457	0.549
P_sp.	0.633	0.545	0.128	0.096	1	0.034	0.347	0.168	0.711	0.97
P_nov	0.068	0.022	0.016	0.068	0.034	1	0.07	0.05	0.036	0.056
P_ora	0.657	0.824	0.15	0.806	0.347	0.07	1	0.443	0.8	0.497
P_pat	0.842	0.429	0.146	0.329	0.168	0.05	0.443	1	0.265	0.271
P_sho	0.603	0.627	0.14	0.457	0.711	0.036	0.8	0.265	1	0.986
R_fus	0.575	0.619	0.287	0.549	0.97	0.056	0.497	0.271	0.986	1

R_leu	0.623	0.012	0.515	0.03	0.132	0.026	0.028	0.214	0.166	0.255
R_lut	0.778	0.226	0.293	0.447	0.15	0.038	0.523	0.355	0.575	0.375
R_nor	0.852	0.966	0.333	0.804	0.808	0.03	0.872	0.393	0.996	0.77
R_rat	0.633	0.727	0.405	0.475	0.794	0.02	0.587	0.389	0.94	0.796
R_sor	0.695	0.309	0.192	0.232	0.545	0.016	0.451	0.355	0.81	0.511
R_tun	0.607	0.098	0.14	0.142	0.305	0.008	0.349	0.405	0.257	0.16
R_vil	0.545	0.435	0.164	0.13	0.657	0.014	0.477	0.345	0.553	0.371
U_cau	0.948	0.894	0.816	0.84	0.938	0.291	0.874	0.938	0.904	0.912
X_myo	0.136	0.066	0.01	0.064	0.142	0.004	0.054	0.263	0.036	0.136
Z_arg	0.633	0.102	0.307	0.361	0.547	0.026	0.321	0.23	0.974	0.988
Z_ped	0.483	0.351	0.25	0.106	0.665	0.078	0.371	0.18	0.946	1

	R_leu	R_lut	R_nor	R_rat	R_sor	R_tun	R_vil	U_cau	X_myo	Z_arg
C_pen	0.483	0.633	0.619	0.749	0.541	0.561	0.467	0.84	0.238	0.752
H_chr	0.092	0.026	0.022	0.078	0.046	0.078	0.044	0.888	0.277	0.086
L_con	0.098	0.058	0.128	0.257	0.07	0.08	0.13	0.93	0.176	0.046
L_for	0.008	0.024	0.585	0.172	0.042	0.124	0.086	0.8	0.01	0.02
M_bur	0.192	0.78	0.988	0.852	0.912	0.82	0.938	0.946	0.076	0.341
M_cap	0.138	0.421	0.998	0.814	0.585	0.164	0.263	0.908	0.078	0.75
M_cer	0.118	0.339	0.976	0.77	0.481	0.062	0.285	0.906	0.072	0.888
M_fus	0.425	0.677	0.758	0.699	0.575	0.375	0.212	0.842	0.046	0.331
M_gou	0.246	0.309	0.116	0.096	0.186	0.152	0.118	0.856	0.437	0.621
M_mus	0.062	0.024	0.138	0.144	0.028	0.032	0.052	0.653	0.008	0.1
N_ale	0.032	0.146	0.938	0.523	0.265	0.397	0.144	0.886	0.136	0.222
N_cer	0.052	0.106	0.09	0.138	0.118	0.072	0.032	0.822	0.232	0.076
N_fus	0.034	0.05	0.236	0.467	0.305	0.355	0.663	0.966	0.792	0.014
N_mit	0.104	0.579	0.98	0.75	0.651	0.271	0.355	0.866	0.124	0.563
P_apo	0.018	0.054	0.2	0.032	0.048	0.058	0.038	0.601	0.022	0.042
P_aus	0.176	0.218	0.996	0.93	0.643	0.393	0.691	0.952	0.096	0.138
P_del	0.349	0.325	0.363	0.541	0.373	0.297	0.403	0.78	0.038	0.148
P_des	0.623	0.778	0.852	0.633	0.695	0.607	0.545	0.948	0.136	0.633
P_gra	0.012	0.226	0.966	0.727	0.309	0.098	0.435	0.894	0.066	0.102
P_her	0.515	0.293	0.333	0.405	0.192	0.14	0.164	0.816	0.01	0.307
P_hig	0.03	0.447	0.804	0.475	0.232	0.142	0.13	0.84	0.064	0.361
P_sp.	0.132	0.15	0.808	0.794	0.545	0.305	0.657	0.938	0.142	0.547
P_nov	0.026	0.038	0.03	0.02	0.016	0.008	0.014	0.291	0.004	0.026
P_ora	0.028	0.523	0.872	0.587	0.451	0.349	0.477	0.874	0.054	0.321
P_pat	0.214	0.355	0.393	0.389	0.355	0.405	0.345	0.938	0.263	0.23
P_sho	0.166	0.575	0.996	0.94	0.81	0.257	0.553	0.904	0.036	0.974
R_fus	0.255	0.375	0.77	0.796	0.511	0.16	0.371	0.912	0.136	0.988
R_leu	1	0.423	0.112	0.693	0.427	0.04	0.152	0.942	0.118	0.301
R_lut	0.423	1	0.353	0.725	0.904	0.403	0.23	0.944	0.058	0.693
R_nor	0.112	0.353	1	0.615	0.681	0.719	0.325	0.896	0.078	0.984

R_rat	0.693	0.725	0.615	1	0.984	0.91	0.884	0.958	0.226	0.776
R_sor	0.427	0.904	0.681	0.984	1	0.916	0.591	0.966	0.136	0.483
R_tun	0.04	0.403	0.719	0.91	0.916	1	0.888	0.976	0.134	0.096
R_vil	0.152	0.23	0.325	0.884	0.591	0.888	1	0.982	0.174	0.269
U_cau	0.942	0.944	0.896	0.958	0.966	0.976	0.982	1	0.984	0.9
X_myo	0.118	0.058	0.078	0.226	0.136	0.134	0.174	0.984	1	0.02
Z_arg	0.301	0.693	0.984	0.776	0.483	0.096	0.269	0.9	0.02	1
Z_ped	0.557	0.794	0.754	0.794	0.723	0.198	0.561	0.898	0.074	0.86

Pairwise *p* value comparisons with significant values (alpha = 0.01) indicated in red. Out of 703 unique comparisons, 9 static allometric slopes significantly differ.

Table S5: Evolutionary allometry phylogenetic ANCOVA

	df	SS	MS	R_2	F	Z	Pr(>F)
log(size)	1	0.016	0.016	0.407	25.148	5.355	0.002
clade	7	0.003	0	0.087	0.771	-1.06	0.856
log(size):clade	5	0.005	0.001	0.134	1.656	2.222	0.02
Residuals	23	0.015	0.001	0.372			
Total	36	0.039					

The phylogenetic equivalent of table 2, where the ANCOVA takes the phylogenetic structure of the data into account. Abbreviations as in table 1.

Table S6: Pairwise analysis of shape evolution rates

	Non-specialist	Frugivore	Folivore	Carnivore	Hopping
Non-specialist	-	4.55	3.09	2.49	1.1
Frugivore	0.02	-	1.47	1.83	4.13
Folivore	0.02	1	-	1.24	2.8
Carnivore	0.499	1	1	-	2.26
Hopping	1	0.02	0.08	1	-

Upper triangle reports pairwise comparisons of shape evolution rates (non-specialists having the slowest overall rate) between non-specialists and different groups of non-specialists. The *compare.evol.rates* function from *geomorph* uses the phylogeny and the shape coordinates to compute these rate analyses. The lower triangle reports the p values for each rate, after correction by the Bonferroni method.

Figure S1: Landmark placements

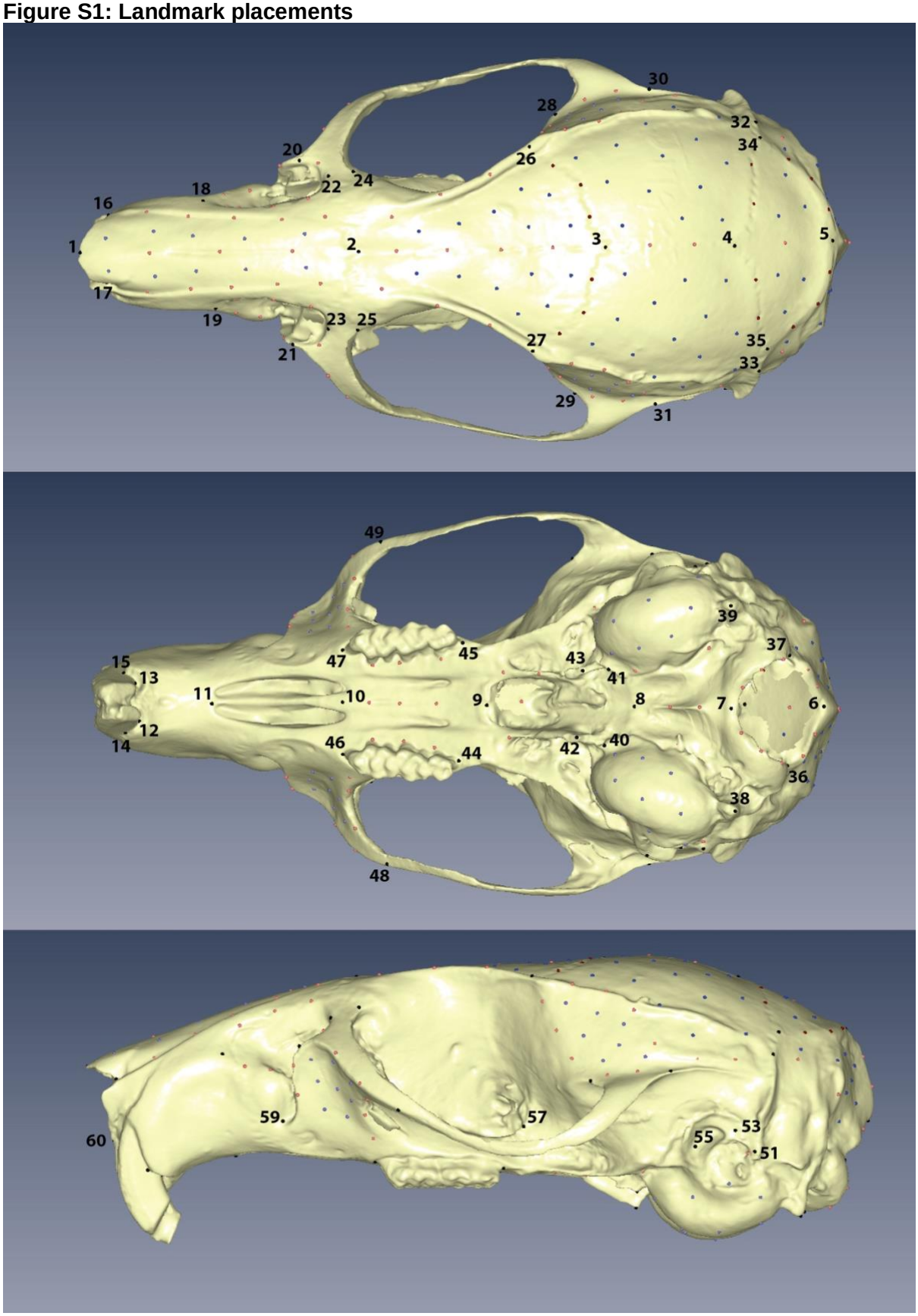

Locations of fixed landmarks (black and numbered), curve semi-landmarks (pink), and patch semi-landmarks (purple) on dorsal, ventral, and lateral views of a representative specimen of Australian rodent. Definitions are given in table S2.

Figure S2: Randomized phylogenetic rarefaction

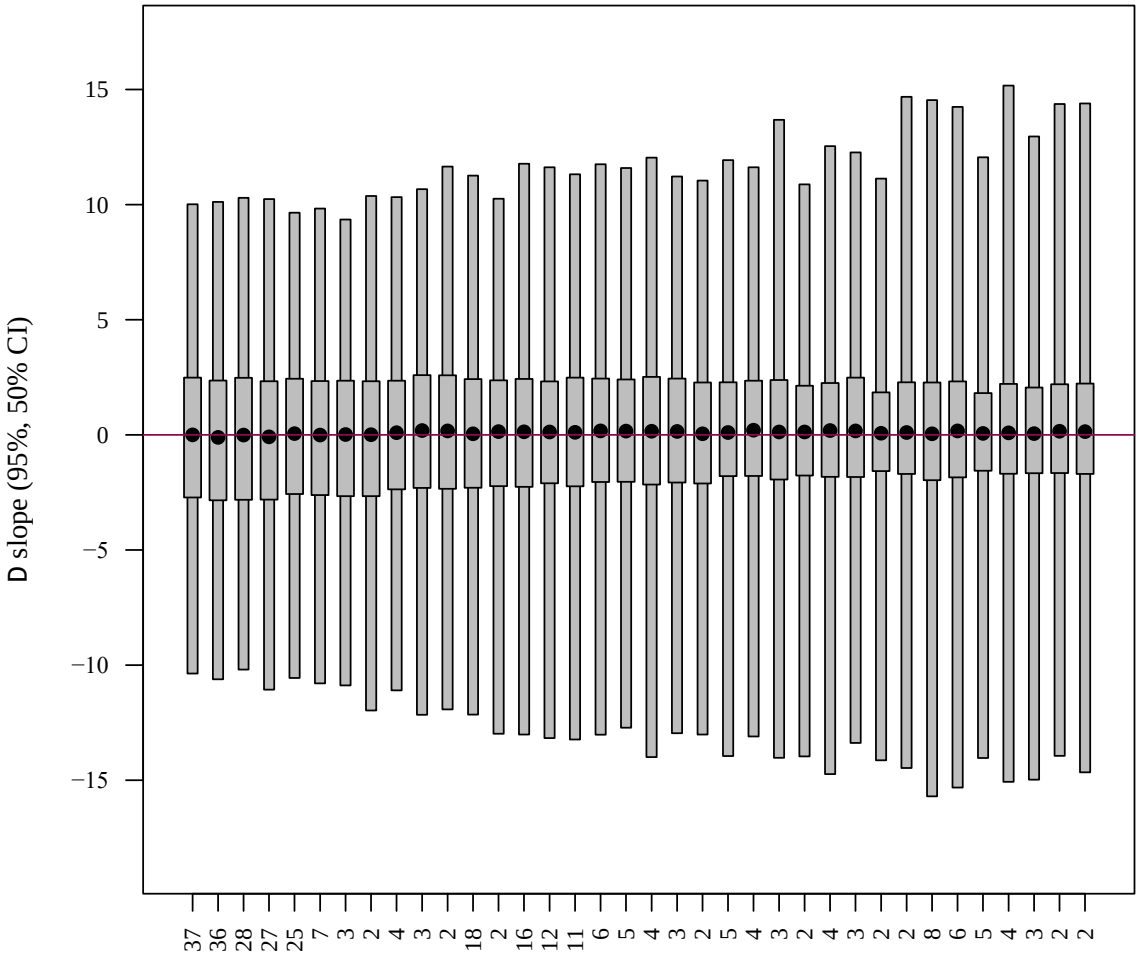

A statistical check to ensure that results from figure 3, which found no impact of sample size on static allometry slope, was not an artifact of phylogenetic relationships. This analysis randomized species into bins with the same number of species as each of the clades in the phylogeny and performed the same rarefaction analysis as in figure 3 for 100 different species randomizations. The graph above gives the confidence intervals for slope change averaged over those 100 randomization and rarefaction steps.